HHS Public Access

Author manuscript

*Nat Med*. Author manuscript; available in PMC 2018 May 13.

Published in final edited form as:

*Nat Med*. 2017 December ; 23(12): 1454–1465. doi:10.1038/nm.4429.

# UCP1-independent signaling involving SERCA2b-mediated calcium cycling regulates beige fat thermogenesis and systemic glucose homeostasis

**Kenji Ikeda**[1,2,3], **Qianqian Kang**[1,2,3], **Takeshi Yoneshiro**[1,2,3], **Joao Paulo Camporez**[4], **Hiroko Maki**[5], **Mayu Homma**[5], **Kosaku Shinoda**[1,2,3], **Yong Chen**[1,2,3], **Xiaodan Lu**[1,2,3], **Pema Maretich**[1,2,3], **Kazuki Tajima**[1,2,3], **Kolapo M. Ajuwon**[6], **Tomoyoshi Soga**[5], and **Shingo Kajimura**[1,2,3]

[1]UCSF Diabetes Center, San Francisco, CA

[2]Eli and Edythe Broad Center of Regeneration Medicine and Stem Cell Research, University of California, San Francisco, CA

[3]Department of Cell and Tissue Biology, University of California, San Francisco, CA

[4]Yale University School of Medicine, Department of Medicine and Cellular & Molecular Physiology, New Haven, CT

[5]Institute for Advanced Biosciences, Keio University, Yamagata, Japan

[6]Department of Animal Sciences, Purdue University, West Lafayette, IN

## Abstract

Uncoupling Protein 1 (UCP1) plays a central role in non-shivering thermogenesis in brown fat; however, its role in beige fat remains unclear. Here we report a robust UCP1-independent thermogenic mechanism in beige fat that involves enhanced ATP-dependent $Ca^{2+}$ cycling by sarco/endoplasmic reticulum $Ca^{2+}$-ATPase2b (SERCA2b) and ryanodine receptor 2 (RyR2). Inhibition of SERCA2b impairs UCP1-independent beige fat thermogenesis in humans and mice, as well as in pigs, a species that lacks a functional UCP1 protein. Conversely, enhanced $Ca^{2+}$ cycling by the activation of α1/β3-adrenergic receptors or the SERCA2b-RyR2 pathway stimulates UCP1-independent thermogenesis. In the absence of UCP1, beige fat dynamically expends glucose through enhanced glycolysis, tricarboxylic acid metabolism, and pyruvate dehydrogenase activity for ATP-dependent thermogenesis by the SERCA2b pathway; beige fat thereby functions as a “glucose-sink” and improves glucose tolerance independent of body-weight



Correspondence and Lead contact: Shingo Kajimura, Ph.D., University of California, San Francisco, UCSD Diabetes Center, Department of Cell and Tissue Biology, San Francisco, CA 94143-0669, Tel: 415-476-9644, shingo.kajimura@ucsf.edu.

**Author contributions**

K.I. and S.K. conceived the study and designed experiments. K.I., Q.K., T.Y., Y. C., X. L., P.M., K.T. and S.K. performed experiments. J.P.C. performed mouse metabolic studies. H.M., M.H., and T.S. performed metabolomics. K.S. performed bioinformatics analyses. K.M.A. contributed pig cell line generation. K.I., Q.K., T.Y., J.P.C. T.S., and S.K. analyzed and interpreted the data. K.I. and S.K. wrote the manuscript. K.I., P.M., and S.K. edited the manuscript.

**Competing Financial Interests**

The authors declare no competitive financial interests.

loss. Our study uncovers a non-canonical thermogenic mechanism by which beige fat controls whole-body energy homeostasis through $Ca^{2+}$ cycling.

**Keywords**

Non-canonical thermogenesis; Obesity; Diabetes; Brown adipose tissue; Beige fat; Calcium cycling; UCP1; SERCA2

## Introduction

UCP1 is a mitochondrial protein specific to brown adipose tissue (BAT), and it uncouples cellular respiration and mitochondrial ATP synthesis to dissipate energy in the form of heat. As UCP1 has been considered the sole “thermogenin” responsible for BAT thermogenesis[1,2], the prevailing dogma is that the action of UCP1 primarily mediates the functions of brown and beige fat, which when activated promote anti-obesity and anti-diabetic effects.

Beige adipocytes are the inducible form of thermogenic fat cells that emerge within white adipose tissue (WAT) following a variety of external stimuli, such as chronic cold exposure, long-term treatment with PPARγ agonists, cancer cachexia, and bariatric surgery[3]. Similar to brown adipocytes, beige adipocytes possess multilocular lipid droplets and thermogenic capacity[4–8], but beige fat in the subcutaneous WAT express lower levels of UCP1 when compared to BAT in mice. Accordingly, beige fat was thought to play a marginal role in the regulation of whole-body energy metabolism[9]. However, several lines of evidence suggest significant biological roles of beige fat. For instance, earlier works demonstrated that obese-resistant mouse strains possess higher amounts of UCP1-positive adipocytes in WAT relative to obese-prone strains[10,11]. It has been also shown that the selective activation of beige adipocyte biogenesis by genetic and pharmacological means sufficiently increases whole-body energy expenditure and protects animals from diet-induced obesity and glucose intolerance[12–15]. Conversely, depletion of beige adipocytes by the adipocyte-specific deletion of *Prdm16* or its co-factor *Ehmt1* causes diet-induced obesity and insulin resistance[16,17]. Of note, the inguinal WAT of cold-acclimated *Ucp1*−/− mice exhibit increased oxygen consumption in response to succinate supplementation[18]. Furthermore, chronic treatment with a β3-adrenergic receptor (β3-AR) agonist increases the metabolic rate of the epididymal WAT of *Ucp1*−/− mice[19]. Recent studies also reported non-shivering thermogenic mechanisms by skeletal muscle thorough sarcolipin[20,21] and by brown and beige fat through a creatine-driven substrate cycle[22]. These results collectively indicate the existence of UCP1-independent thermogenesis; however, the underlying mechanisms and its physiological significance of UCP1-independent roles in beige fat remain poorly understood. Here, we report $Ca^{2+}$ cycling as an UCP1-independent thermogenic mechanism in beige fat that controls whole-body energy homeostasis.

## Results

### UCP1 is dispensable for beige fat thermogenesis *in vivo*

We previously reported that adipose tissue-selective transgenic expression of *Prdm16* driven by the *Fabp4* promoter and enhancer potently promoted beige adipocyte biogenesis in the subcutaneous WAT, whereas it caused no morphological or molecular changes in the interscapular BAT (iBAT) and the epididymal WAT depots[12]. To examine the requirement of UCP1 for beige adipocyte function *in vivo*, we crossed *Fabp4-Prdm16* transgenic mice (*Prdm16* Tg) with *Ucp1*−/− mice in the Bl6 background (*Prdm16* Tg x *Ucp1*−/−). First, we confirmed that the *Prdm16* transgene was selectively and equally expressed in the adipose tissues of *Prdm16* Tg mice and *Prdm16* Tg x *Ucp1*−/− mice (Supplementary Fig. 1a,b). *Prdm16* Tg mice expressed significantly higher levels of *Ucp1* in the inguinal WAT, but not in the iBAT and the epididymal WAT, than the littermate controls (Supplementary Fig. 1c). Expression of the brown and beige fat-selective genes and mitochondrial genes was also higher in the inguinal WAT of *Prdm16* Tg mice than the controls (Supplementary Fig. 1d). Similarly, the inguinal WAT of *Prdm16* Tg x *Ucp1*−/− mice expressed higher mRNAs of the brown and beige fat-selective genes except *Ucp1* compared to the littermate *Ucp1*−/− mice (Supplementary Fig. 1d). No significant change was seen in the brown and beige fat-selective gene expression in iBAT and epididymal WAT (Supplementary Fig. 1e,f). The activation of brown and beige fat–selective genes in *Prdm16* Tg mice and *Prdm16* Tg x *Ucp1*−/− mice was accompanied by increased clusters of multilocular adipocytes in the inguinal WAT (Supplementary Fig. 1g). In the iBAT, brown adipocytes from *Ucp1*−/− mice and *Prdm16* Tg x *Ucp1*−/− mice contained larger lipid droplets relative to *Ucp1*+/+ animals (Supplementary Fig. 1h). No noticeable change was observed in the morphology of iBAT and epididymal WAT by *Prdm16* transgenic expression (Supplementary Fig. 1h,i). Accordingly, this animal model provides valuable insights regarding the extent to which the physiological function of beige fat in whole-body energy metabolism is mediated by the action of UCP1.

Upon cold exposure at 6°C, *Prdm16* Tg and the littermate control mice maintained their core body temperature (Fig. 1a). Consistent with the previous studies[1,23], *Ucp1*−/− mice showed a severe impairment in cold tolerance; however, the body weight-matched *Prdm16* Tg x *Ucp1*−/− mice were capable of maintaining their core body temperature under cold conditions (Fig. 1b). *Prdm16* Tg mice displayed modestly but significantly higher oxygen consumption rate ($VO_2$) and heat production (kcal) compared to the control mice following cold exposure at 6 °C (Fig. 1c,d), though there was no difference in energy expenditure at 30°C (Supplementary Fig. 2a). Notably, $VO_2$ and heat generation in *Prdm16* Tg x *Ucp1*−/− mice were significantly higher than those in the littermate *Ucp1*−/− mice at 6°C (Fig. 1e,f). During cold exposure, no significant difference was observed in either food intake or locomotor activity among the genotypes (Supplementary Fig. 2b,c).

To determine the specific tissues responsible for thermogenesis in *Prdm16* Tg x *Ucp1*−/− mice, we next monitored the tissue temperature in iBAT, inguinal WAT, and skeletal muscle following norepinephrine (NE) treatment (Fig. 1g). The iBAT temperature of *Prdm16* Tg mice and the littermate control mice increased by 1.0°C or higher following NE treatment,

whereas such an increase was not observed in *Ucp1*−/− mice and *Prdm16* Tg x *Ucp1*−/− mice (Fig. 1h). On the other hand, the inguinal WAT temperature in *Prdm16* Tg x *Ucp1*−/− mice significantly increased, comparable to the increase in iBAT, following NE treatment. In skeletal muscle, no increase in tissue temperature was seen. We also found that oxygen consumption rate (OCR) of iBAT was significantly increased by NE in *Prdm16* Tg mice and the control mice, but not in *Ucp1*−/− and *Prdm16* Tg x *Ucp1*−/− mice (Supplementary Fig. 2d). In contrast, OCR in the inguinal WAT of *Prdm16* Tg and *Prdm16* Tg x *Ucp1*−/− mice was significantly higher than their respective controls following NE treatment (Supplementary Fig. 2e). In epididymal WAT, no significant change was seen among the genotypes (Supplementary Fig. 2f). Of note, the contribution of skeletal muscle shivering appears negligible in the quantification of heat generation in this mouse model because electromyography found no difference in muscle shivering between *Prdm16* Tg x *Ucp1*−/− mice and *Ucp1*−/− mice both at 30°C and 6°C (Fig. 1i,j). We also observed no difference in serum concentration of creatine kinase, a marker of muscle damage between the two groups after cold exposure (Supplementary Fig. 2g).

## SERCA2b controls UCP1-independent thermogenesis in beige adipocytes

To investigate the mechanisms of UCP1-independent thermogenesis in *Prdm16* Tg x *Ucp1*−/− mice, we performed RNA-sequencing analysis of the inguinal WAT, followed by Metascape pathway analysis[24]. We identified 391 genes that were significantly ($P < 0.05$) up-regulated in the inguinal WAT of *Prdm16* Tg mice and *Prdm16* Tg x *Ucp1*−/− mice (Fig. 2a). We also found 640 genes that were selectively elevated in *Prdm16* Tg x *Ucp1*−/− mice relative to the other genotypes. The Metascape pathway analysis found that the commonly up-regulated pathways in *Prdm16* Tg mice and *Prdm16* Tg x *Ucp1*−/− mice were linked to PPAR signaling, fatty acid metabolism, and brown fat differentiation, many of which are involved in beige adipocyte biogenesis (Fig. 2b). On the other hand, several metabolic pathways, including tricarboxylic acid (TCA) metabolism, branched-chain amino acid (BCAA) oxidation, and glycolysis, were uniquely up-regulated in *Prdm16* Tg x *Ucp1*−/− mice compared to the other genotypes. Notably, the pathway linking to “cardiac muscle contraction” was uniquely up-regulated in *Prdm16* Tg x *Ucp1*−/− mice; mRNA expression of several cardiac muscle-related genes involving in $Ca^{2+}$ cycling, including *Serca2* and ryanodine receptor 2 (*Ryr2*), were significantly higher in *Prdm16* Tg x *Ucp1*−/− mice than the other groups (Fig. 2c). The changes in $Ca^{2+}$ cycling-related genes caught our attention because mutations in the *RyR1* gene cause malignant hyperthermia in humans and pigs[25,26] and that sarcolipin, a SERCA1 regulator, is required for non-shivering thermogenesis in the skeletal muscle[20,21].

SERCA2b, one of the isoforms of SERCA2 encoded by the *Atp2a2* gene, is the dominant form in beige adipocytes; mRNA expression of *Serca2b* was much higher than *Serca1* (a skeletal muscle-selective form of SERCA), *Serca2a*, and *Serca3* (Fig. 2d). *SERCA2b* is also the dominant form of SERCA in differentiated human beige adipocytes[27] (Fig. 2e). Of note, *Serca2b* mRNA expression in the inguinal WAT was increased by chronic cold exposure at 4°C for 7 days (Supplementary Fig. 3a). SERCA2 protein expression was also increased by cold exposure in the inguinal WAT, whereas such change was not observed in the iBAT (Supplementary Fig. 3b). Immunohistochemistry in beige adipocytes showed that SERCA2

was localized in the endoplasmic reticulum (ER), based on its co-localization with a marker of the ER and sarcoplasmic reticulum (SR), calnexin (Supplementary Fig. 3c).

Since NE from sympathetic nerves is known to activate the β3-adrenoceptor (β3-AR) and trigger intracellular cAMP signaling[28], we examined whether SERCA2 expression was regulated by the cAMP pathway. To this end, primary beige adipocytes were treated with forskolin, an adenylyl cyclase activator that generates cAMP. We found that forskolin treatment for 4 hours significantly increased *Serca2b* mRNA expression, while it did not alter other forms of *Serca* in mice and human beige adipocytes (Fig. 2d,e). Because expression of *Ucp2* and *Ucp3* in the inguinal WAT did not differ among the four genotypes (Supplementary Fig. 3d,e) and mitochondria patch-clamp recordings showed that proton current in the mitochondrial membrane of brown and beige fat is highly UCP1-dependent[29,30], UCP1-independent thermogenesis in the inguinal WAT of *Prdm16* Tg x *Ucp1−/−* mice likely occurred through a mechanism independent of mitochondrial proton uncoupling.

Next, we aimed to determine the requirement of SERCA2b-mediated $Ca^{2+}$ cycling for UCP1-independent thermogenesis. To this end, we established *Ucp1*−/− beige adipocytes by differentiating the immortalized stromal vascular fractions (SVFs) from the inguinal WAT of *Prdm16* Tg x *Ucp1*−/− mice. NE treatment significantly increased basal and oligomycin-resistant cellular OCR in *Ucp1*−/− beige adipocytes by 70% and 78%, respectively (Fig. 2f). Acute inhibition of SERCA2 by a pharmacological SERCA inhibitor, thapsigargin, for one hour completely blunted the NE-induced cellular respiration (Fig. 2f). Next, we utilized the CRISPR-Cas9 system to introduce homozygous null mutations in *Atp2a2* in *Ucp1*−/− beige adipocytes (Fig. 2g). We confirmed with immunohistochemistry that the SERCA2 protein was abundantly expressed in beige adipocytes expressing a scrambled guide RNA, whereas it was not detected in the *Atp2a2−/−* cells (Fig. 2h). Genetic deletion of *Atp2a2* in *Ucp1*−/− beige adipocytes significantly reduced basal and NE-stimulated OCR compared to the control cells (Fig. 2i). Furthermore, acute inhibition of SERCA by thapsigargin for one hour reduced NE-induced OCR in control cells, whereas the inhibitory effect was not observed in *Atp2a2−/−;Ucp1−/−* cells (Fig. 2i). The requirement of SERCA2 for beige fat thermogenesis was confirmed in two independent clonal cell lines (Supplementary Fig. 4a,b).

As an alternative approach, we used lentiviruses expressing a scrambled control RNA or shRNAs targeting *Atp2a2* to deplete endogenous SERCA2b in beige adipocytes (Supplementary Fig. 4c). We found that depletion of SERCA2b by two distinct shRNAs significantly reduced NE-stimulated OCR in *Ucp1*−/− beige adipocytes (Supplementary Fig. 4d). SERCA2b depletion also reduced oligomycin-resistant respiration, but not FCCP-stimulated respiration in *Ucp1*−/− beige adipocytes (Supplementary Fig. 4d). Because SERCA2b depletion similarly blunted NE-induced OCR in wild-type beige adipocytes (Supplementary Fig. 4e), SERCA2b is required for beige fat thermogenesis both in the presence and absence of UCP1. The SERCA2b pathway also plays an important role in human beige adipocytes: NE treatment significantly increased OCR in *UCP1*−/− human beige adipocytes, whereas the NE effect was completely blunted by thapsigargin (Supplementary Fig. 5a,b).

Next, we employed a gain-of-function approach to determine the role of SERCA2b in UCP1-independent thermogenesis. To this end, we overexpressed SERCA2b in *Ucp1*−/− beige adipocytes by infecting the cells with a low titer of lentivirus expressing SERCA2b or an empty vector (Supplementary Fig. 5c,d). We found that a modest elevation of *Serca2b* mRNA expression by approximately 1.7-fold, an equivalent degree of increase found in *Prdm16* Tg x *Ucp1*−/− mice (see Fig. 2c), led to a significant increase in $Ca^{2+}$ release from the ER in response to NE treatment, likely due to enhanced $Ca^{2+}$ loading to the ER (Supplementary Fig. 5e). This increase was accompanied by enhanced thermogenesis following NE treatment (Fig. 2j).

Based on the above results, we examined the genetic requirement of SERCA2b for beige fat thermogenesis *in vivo*. To this end, we crossed *Atp2a2*$^{flox/flox}$ mice with *Adiponectin*-Cre mice (Adipo-*Atp2a2*−/−) and found that *Serca2b* mRNA was significantly lower in the adipose tissues of Adipo-*Atp2a2*−/− mice than the littermate controls, but not in the heart (Supplementary Fig. 6a). The partial reduction in *Serca2b* expression in the adipose tissues is likely due to the expression of *Serca2b* in other non-adipocytes within the tissues. We also found no difference in the expression of UCP1 and mitochondrial proteins between Adipo-*Atp2a2*−/− and the control mice at 22°C (Supplementary Fig. 6b–e). Histological examination of the adipose tissues identified no obvious abnormality in the cell/tissue structure and the mitochondrial morphology in Adipo-*Atp2a2*−/− mice (Supplementary Fig. 6f,g). Under a regular diet at 22°C, we observed no difference in body weight, adipose tissue mass, and food intake between Adipo-*Atp2a2*−/− mice and the controls (Supplementary Fig. 6h–j). However, the inguinal WAT of Adipo-*Atp2a2*−/− mice displayed significantly lower OCR than the littermate controls following NE treatment (Fig. 2k), suggesting that SERCA2b is required for beige fat thermogenesis. On the other hand, NE potently increased OCR in the iBAT of Adipo-*Atp2a2*−/− to a similar degree as the control mice (Fig. 2l), indicating that SERCA2 is dispensable for BAT thermogenesis in the presence of UCP1. This is consistent with the results that pharmacological inhibition of SERCA by thapsigargin did not attenuate NE-induced OCR in wild-type brown adipocytes, whereas *Ucp1*−/− brown adipocytes failed to respond to NE (Supplementary Fig. 6k).

To further probe the requirement of SERCA2b for adipose thermogenesis *in vivo*, we recorded the adipose tissue temperature of Adipo-*Atp2a2*−/− mice. To induce beige adipocyte biogenesis pharmacologically, we chronically treated the mice with CL316,243 for five consecutive days. We found that the inguinal WAT temperature of control mice rapidly increased by 1.0°C or higher following NE treatment, a reflection of beige fat thermogenesis. However, the NE-induced beige fat thermogenesis was completely blunted in Adipo-*Atp2a2*−/− mice (Fig. 2m). In contrast, the iBAT temperature was significantly induced by NE injection both in Adipo-*Atp2a2*−/− mice and the controls (Fig. 2n). No difference in skeletal muscle temperature was seen between the two groups (Fig. 2o and Supplementary Fig. 6l).

## Enhanced $Ca^{2+}$ cycling stimulates UCP1-independent thermogenesis in beige fat

Given the established role of SERCA in intracellular $Ca^{2+}$ cycling, we examined the extent to which $Ca^{2+}$ flux controls UCP1-independent thermogenesis. We observed a robust

increase in intracellular $Ca^{2+}$ levels both in wild-type and *Ucp1*−/− beige adipocytes within one minute following NE treatment (Fig. 3a). Of note, depletion of extracellular $Ca^{2+}$ did not affect NE-induced respiration in *Ucp1*−/− beige adipocytes (Fig. 3b), whereas acute depletion of intracellular $Ca^{2+}$ by a cell-permeant $Ca^{2+}$ chelator, BAPTA, completely blocked NE-induced OCR both in wild-type and *Ucp1*−/− beige adipocytes (Fig. 3c and Supplementary Fig. 7a). On the other hand, brown fat thermogenesis was highly dependent on UCP1 and not affected by BAPTA (Fig. 3d).

NE is known to binds to β-ARs but also to α-adrenergic receptors (α-ARs) and triggers intracellular $Ca^{2+}$ signaling[31]. Since our RNA-seq analysis found α1-AR, β1-AR, and β3-AR were highly expressed in the inguinal WAT of *Prdm16* Tg x *Ucp1*−/− mice (Supplementary Fig. 7b), we asked which forms of ARs mediate the stimulatory effect of NE on UCP1-independent thermogenesis. We found that α1-AR and β3-AR mediate the action of NE to activate UCP1-independent thermogenesis as pharmacological stimulation of α1-AR and β3-AR by phenylephrine and CL316,243, respectively, significantly increased OCR and intracellular $Ca^{2+}$ levels in *Ucp1*−/− beige adipocytes (Fig. 3e and Supplementary Fig. 7c). On the other hand, the β1-AR agonist (denopamine) and α2-AR agonist (clonidine) did not alter OCR. The lack of the α2-AR agonist effect is likely because α2-AR is expressed at an undetectable level in beige adipocytes (Supplementary Fig. 7b). Conversely, pharmacological inhibition of α1-AR and β3-AR by phenoxybenzamine and SR59230A, respectively, partially but significantly blunted the NE-stimulated OCR in *Ucp1*−/− beige adipocytes (Fig. 3f).

We next employed the following gain-of-function approaches to test whether enhanced $Ca^{2+}$ cycling through the SERCA2b-RyR2 pathway stimulates UCP1-independent thermogenesis. First, we examined the extent to which enhanced $Ca^{2+}$ flux through RyR2 stimulates beige fat thermogenesis. The rationale is based on our RNA-seq data that *Ryr2* expression was significantly higher in the inguinal WAT of *Prdm16* Tg x *Ucp1*−/− mice relative to the other genotypes (Supplementary Fig. 8a). Since RyR2 is the major form among the ryanodine receptor family members in beige adipocytes (Supplementary Fig. 8b), we overexpressed RyR2 or an empty vector in *Ucp1*−/− beige adipocytes (Supplementary Fig. 8c,d). While RyR2 overexpression did not affect beige adipocyte differentiation or mitochondrial contents (Supplementary Fig. 8e), *Ucp1*−/− beige adipocytes expressing RyR2 displayed higher OCR relative to the vector-expressing cells (Fig. 3g). Furthermore, overexpression of SERCA2b and RyR2 additively increased NE-stimulated OCR in *Ucp1*−/− beige adipocytes (Supplementary Fig. 8f). Additionally, pharmacological inhibition of RyR2 by ryanodine at a high dose (100 μM) or ruthenium red partially but significantly blunted NE-stimulated OCR (Supplementary Fig. 8g,h). Second, we overexpressed Calstabin2 (encoded by *Fkbp1b*), a key subunit of the RyR2 complex, in *Ucp1*−/− beige adipocytes (Supplementary Fig. 8i). Previous studies demonstrated that Calstabin2 overexpression in cardiomyocytes reduces $Ca^{2+}$ leak and increases $Ca^{2+}$ loading in the SR, thereby enhances $Ca^{2+}$ release and muscle contractility in response to caffeine stimulation[32–34]. Of note, Calstabin2 is abundantly expressed in the adipose tissue (Supplementary Fig. 8j), although its mRNA expression was unchanged by *Prdm16* transgenic expression (Supplementary Fig. 8k). We found that Calstabin2 overexpression in *Ucp1*−/− beige adipocytes potentiated $Ca^{2+}$ release from the ER following NE treatment (Fig. 3h). The enhanced $Ca^{2+}$ release in the Calstabin2-

expressing cells was accompanied by a significant increase in NE-induced OCR relative to the vector-expressing cells (Fig. 3i). Third, we tested whether acute enhancement of the RyR2 function by a pharmacological stabilizer of RyR2 (S107) activates UCP1-independent thermogenesis *in vivo*. S107 treatment is known to prevent $Ca^{2+}$ leak and enhance $Ca^{2+}$ loading in the SR by stabilizing the interaction between Calstabin2 and RyR2, leading to an improvement in cardiac contractility *in vivo*[35]. S107 treatment also enhances caffeine-induced $Ca^{2+}$ release from the ER and promotes insulin secretion in pancreatic beta cells[36]. Accordingly, we implanted osmotic pumps each containing S107 at a dose of 20 mg $kg^{-1}$ or vehicle in *Ucp1*−/− mice for seven days and afterward transferred the mice to 6°C. Although the vehicle-treated *Ucp1*−/−mice developed hypothermia following cold exposure, the S107-treated *Ucp1*−/− mice were capable of maintaining core body temperature (Fig. 3j). Since muscle shivering in *Ucp1*−/− mice was already active under cold, we did not observe any further enhancement in muscle shivering by S107 (Fig. 3k).

A recent study reported a futile cycle of creatine-driven thermogenesis in brown and beige fat[22]. Because both $Ca^{2+}$ cycling and creatine cycling involve ATP-dependent thermogenesis, we examined the extent to which the two mechanisms converge to control UCP1-independent thermogenesis. To this end, we depleted SERCA2b in *Ucp1*−/− beige adipocytes by the lentiviral shRNA and inhibited the creatine cycle by treating the cells with β-guanidinopropionic acid (β-GPA), a creatine analog that potently inhibits creatine transport. We found that SERCA2b depletion significantly reduced OCR in *Ucp1*−/− beige adipocytes even in the presence of β-GPA treatment, while inhibition of OCR by β-GPA was not observed in the SERCA2b-depleted cells (Supplementary Fig. 8l).

## The anti-obesity and anti-diabetic effects of beige fat are independent of UCP1

The distinct function of the SERCA2b-RyR2 pathway in UCP1-independent thermogenesis led us to hypothesize that the activation of beige adipocyte biogenesis could prevent diet-induced obesity and glucose intolerance independent of UCP1. To test this hypothesis, *Prdm16* Tg x *Ucp1*−/− mice and the controls were subjected to a high-fat diet (HFD) for up to 24 weeks. We found that *Prdm16* Tg mice gained significantly less body weight at 19 weeks of HFD and thereafter under the ambient temperature at 22°C (Fig. 4a). *Prdm16* Tg x *Ucp1*−/− mice also gained significantly less body weight than the littermate *Ucp1*−/− mice at 10 weeks of HFD and thereafter (Fig. 4b). The difference in body weight was due to reduced fat mass, but not to lean mass (Supplementary Fig. 9a). Notably, *Prdm16* Tg x *Ucp1*−/− mice fully normalized the obese phenotype to a similar degree as *Prdm16* Tg mice (Fig. 4c). We did not observe any difference in food intake or locomotor activity among the genotypes (Supplementary Fig. 9b,c).

We next probed the requirement of UCP1 for systemic glucose homeostasis. A glucose tolerance test (GTT) showed that *Prdm16* Tg mice exhibited significantly improved glucose tolerance relative to the littermate controls at 10 weeks of HFD feeding, even when there was no difference in body weight between the two groups (Fig. 4d). Similarly, *Prdm16* Tg x *Ucp1*−/− mice displayed a marked increase in glucose tolerance at 10 weeks of HFD feeding relative to the littermate *Ucp1*−/− mice (Fig. 4d). Glucose tolerance of *Prdm16* Tg x *Ucp1*−/− mice was improved to a similar degree to *Prdm16* Tg mice when normalized to their

respective controls (Supplementary Fig. 9d). Similarly, an insulin tolerance test (ITT) found that *Prdm16* mice and *Prdm16* Tg x *Ucp1−/−* were both more insulin sensitive than their respective littermate controls at 11 weeks of HFD feeding (Fig. 4e and Supplementary Fig. 9e). The improvement in GTT and ITT was not observed under a regular chow diet (Supplementary Fig. 9f,g).

When animals were fed HFD under thermoneutrality at 30°C, *Prdm16* Tg mice gained slightly less body weight than the littermate controls (Fig. 4f). The reduced body weight gain in *Prdm16* Tg mice was associated with reduced fat mass, but not with lean mass (Supplementary Fig. 9h). On the other hand, *Prdm16* Tg x *Ucp1−/−* mice and *Ucp1−/−* mice gained a similar degree of body weight and fat mass at 30°C (Fig. 4f and Supplementary Fig. 9i); however, *Prdm16* Tg mice and *Prdm16* Tg x *Ucp1−/−* mice exhibited an improved glucose tolerance relative to the respective littermate controls (Fig. 4g).

## Enhanced glucose utilization in UCP1-null beige fat

To investigate the molecular mechanisms by which beige fat improves systemic glucose tolerance in an UCP1-independent manner, we performed metabolomics in the inguinal WAT (Supplementary Table 1). The metabolomics data combined with the RNA-seq data suggest that glycolysis and the TCA cycle were substantially activated in the inguinal WAT of *Prdm16* Tg x *Ucp1−/−* mice (Fig. 5a, also see Fig. 2b). For instance, mRNA expression of a large number of genes involving in glycolysis and TCA metabolism were significantly higher in *Prdm16* Tg x *Ucp1−/−* mice relative to the other groups (Supplementary Fig. 10a). This alteration was selective in the inguinal WAT because no major difference was seen in the iBAT and the epididymal WAT (Supplementary Fig. 10b c).

The results lead to the hypothesis that *Ucp1*−/− beige adipocytes actively utilize glucose through enhanced glycolysis and TCA metabolism for ATP-dependent thermogenesis by SERCA2b. In fact, glucose uptake in the inguinal WAT of *Prdm16* Tg x *Ucp1−/−* mice was significantly higher relative to the other genotypes (Fig. 5b). In contrast, glucose uptake in the iBAT and the epididymal WAT was not different between *Prdm16* Tg x *Ucp1−/−* mice and the controls. Furthermore, enzymatic activity and gene expression of the pyruvate dehydrogenase (PDH) complex, a key regulator that converts pyruvate into Acetyl-CoA, was significantly higher in the inguinal WAT of *Prdm16* Tg x *Ucp1−/−* mice relative to the other groups (Fig. 5c and Supplementary Fig. 10d). PDH activity in the iBAT and the epididymal WAT was not different between *Prdm16* Tg x *Ucp1−/−* mice and *Ucp1−/−* mice (Fig. 5c). Of note, the enhanced glucose oxidation in *Ucp1*−/− beige fat significantly affects whole-body metabolism; *Prdm16* Tg x *Ucp1−/−* mice displayed higher respiratory exchange ratio (RER, $VO_2/VCO_2$) than the littermate *Ucp1*−/− mice, indicating that *Prdm16* x *Ucp1−/−* mice utilize carbohydrate (glucose) as the primary fuel source rather than fat (Fig. 5d).

## The SERCA2-RyR2 pathway controls glucose oxidation in beige fat

The above results led us to examine the extent to which the SERCA2b-RyR2 pathway controls glucose utilization in beige fat. Accordingly, we measured extracellular acidification rate (ECAR), a cellular index of glycolysis, in differentiated *Ucp1*−/− beige adipocytes under a culture condition with low or high glucose concentrations. We found that

NE treatment potently increased ECAR in *Ucp1*−/− beige adipocytes both under low and high glucose conditions (Fig. 6a). Oligomycin treatment further increased ECAR in *Ucp1*−/− beige adipocytes, whereas blocked glycolysis by 2-Deoxy-D-glucose (2-DG) potently reduced basal and NE-induced ECAR to a similar level.

When SERCA2b was depleted by the lentiviral shRNA targeting *Atp2a2*, we found a significant reduction in basal and NE-stimulated ECAR (Fig. 6b). Acute depletion of intracellular $Ca^{2+}$ by BAPTA completely blocked NE-induced ECAR (Supplementary Fig. 11a), indicating that NE-stimulated $Ca^{2+}$ flux is required for glycolytic ATP production in beige adipocytes. Consistent with the observation, depletion of SERCA2b led to a significantly reduction in glucose oxidation in *Ucp1*−/− beige adipocytes (Fig. 6c). The decreases in ECAR and glucose oxidation by SERCA2b depletion were accompanied by reduced glucose uptake (Fig. 6d). On the other hand, fatty acid oxidation was not affected by SERCA2b depletion (Fig. 6e). Conversely, overexpression of RyR2 significantly increased ECAR and glucose uptake in *Ucp1*−/− beige adipocytes (Fig. 6f and Supplementary Fig. 11b). Glycolytic ATP production profoundly contributes to ATP-dependent thermogenesis in *Ucp1*−/− beige fat because blockade of the glycolysis pathway by 2-DG reduced OCR in *Ucp1*−/− beige adipocytes, while NE potently and quickly increased OCR in the vehicle-treated cells (Fig. 6g).

### The $Ca^{2+}$ cycling thermogenesis is an evolutionally conserved mechanism

Lastly, we asked if the $Ca^{2+}$ cycling-mediated thermogenesis is evolutionally relevant in other mammalian species. To do this, we chose pig adipocytes as a model because pigs lack a functional UCP1 protein due to deletions of exon 3 to 5 of the *Ucp1* gene[37]. Pig SVFs isolated from the subcutaneous WAT of neonatal piglets were infected with retroviruses expressing PRDM16 or an empty vector and differentiated into mature adipocytes under an adipogenic condition (Fig. 6h). We found that PRDM16-expressing pig adipocytes expressed significantly higher mRNA expression of the beige-selective genes, including *Cidea, Dio2, Elovl3,* and *Tmem26,* than the vector-expressing adipocytes (Fig. 6i). The pig beige adipocytes also expressed higher amounts of mitochondrial proteins than the vector-expressing white adipocytes (Fig. 6j). When pig SERCA2b was depleted by the lentiviral shRNA targeting *Atp2a2* (Fig. 6k), we observed a significant reduction in basal and NE-stimulated OCR, whereas NE potently increased OCR in beige adipocytes expressing a scrambled RNA (Fig. 6l). NE treatment also increased ECAR in pig beige adipocytes, whereas SERCA2b depletion reduced basal and NE-stimulated ECAR (Fig. 6m). Conversely, RyR2-expressing pig adipocytes displayed higher OCR than vector-expressing cells (Fig. 6n).

## Discussion

Our results suggest the following model (Fig. 6o). In response to cold exposure, NE binds to α1-AR and β3-AR to increase intracellular $Ca^{2+}$ flux by activating SERCA2b and RyR2 in beige adipocytes. $Ca^{2+}$ is transported back to its storage in the ER by the action of SERCA2b and likely to the mitochondria through voltage-dependent anion channel and mitochondrial calcium uniporter. Increased $Ca^{2+}$ in the mitochondria, in turn, activates

pyruvate dehydrogenase phosphatase PDP1c[38], thereby activating PDH enzyme and ATP synthesis. In the absence of UCP1, beige adipocytes utilize glucose as the primary fuel source for ATP synthesis through enhanced glycolysis, TCA metabolism, and the mitochondrial electron transport chain (ETC). Non-canonical thermogenesis occurs when calcium transport is uncoupled from ATP hydrolysis by SERCA2b, although regulators of SERCA2 activity in beige adipocytes remain undetermined. Because the inhibition of RyR2 partly, but not completely, blocks NE-induced thermogenesis, it is conceivable that inositol 1,4,5-trisphosphate receptors ($IP_3Rs$), such as $IP_3R1$ and $IP_3R2$, are also involved in the regulation of $Ca^{2+}$ release and non-canonical thermogenesis in beige adipocytes. Additionally, PKA signaling is known to phosphorylates RyR2, leading to dissociation between Calstabin2 from RyR2 and enhancing $Ca^{2+}$ release from the SR[39]. NE-induced post-translational modifications of RyR2 and SERCA2b in beige fat await future investigations.

While brown adipocytes are highly enriched in mitochondria, they express very low amounts of the ATP synthase and thus possess low ATP synthesis capacity[40]. As such, ATP-dependent thermogenesis is likely incapable of fully compensating for the UCP1 loss *in vivo*. On the other hand, beige adipocytes express high levels of the ATP synthase and generate ATP through enhanced glycolysis, TCA cycle, and the mitochondrial ETC; thus, the ATP-dependent thermogenesis by SERCA2 can compensate for the UCP1 loss. These data suggest a distinct functional requirement of UCP1-mediated canonical thermogenesis and the SERCA2b-mediated thermogenesis for brown fat and beige fat, respectively.

Our study demonstrates the biological significance of the non-canonical beige fat thermogenesis in whole-body energy metabolism, *i.e.,* activation of beige fat biogenesis by the fat-selective PRDM16 expression protects animals from cold-induced hypothermia and diet-induced obesity and diabetes independent of UCP1. In skeletal muscle, non-shivering thermogenesis occurs by a UCP1-independent mechanism in which sarcolipin controls the SERCA1's ATP hydrolysis activity and $Ca^{2+}$ transport[21]. Tangentially, $Ca^{2+}$ cycling by SERCA1 and RyR1 is suggested to be a mechanism of thermogenesis in the "heat organ" located in the an extraocular muscle beneath the brain of endothermic fish, such as swordfish and blue marlin[41]. These results together with the present study in mice, humans, and pigs indicate that $Ca^{2+}$ cycling thermogenesis is an evolutionally conserved mechanism that controls whole-body energy expenditure and glucose metabolism in the absence of UCP1. The quantitative contribution of canonical thermogenesis by UCP1 versus non-canonical thermogenesis by the UCP1-independent mechanisms to the regulation of whole-body energy metabolism should be determined by characterizing metabolic phenotypes of mice lacking UCP1 and SERCA2b in the adipose tissue.

Brown and beige adipocytes utilize fatty acids as the primary fuel source for thermogenesis by UCP1. In the absence of UCP1, however, we found that beige adipocytes dynamically expend glucose and generate ATP through enhanced glycolysis, TCA metabolism, and PDH activity for ATP-dependent thermogenesis by $Ca^{2+}$ cycling. This metabolic rewiring towards glucose oxidation is highly dependent on the SERCA2b-RyR2 pathway and this enhancement significantly alters whole-body metabolism towards carbohydrate oxidation. Our data indicate that the "glucose sink" function of beige fat underlies the recent

observations, including the present study, that beige fat positively regulates glucose tolerance independent of body-weight loss[12,16,17].

Under pathological conditions such as obesity and diabetes mellitus, fluctuations in $Ca^{2+}$ homeostasis and SERCA2 function have been reported in the liver and the pancreas[36,42,43]. In the adipose tissue, the publically available datasets (*e.g.,* GSE28598, GSE30247, GSE32095) show reduced expression *Serca2* in diet-induced obese mice relative to lean mice, indicating that adipose $Ca^{2+}$ cycling is defective in states of obesity. It has been also reported that mitochondrial-associated ER membrane (MAM), a key structural unit for $Ca^{2+}$ exchange between mitochondria and ER, is dysfunctional in the diabetic liver and that restoration of the MAM integrity by overexpressing a MAM protein, cyclophilin D, or IP3R1 depletion improves insulin signaling[44,45]. Although the MAM function in the adipose tissue under an obese state warrants future investigations, it is conceivable that restoring adipose $Ca^{2+}$ cycling is an effective approach to stimulate non-canonical thermogenesis in beige fat. This is significant because such approach may be effective even in subjects who do not possess appreciable levels of preexisting UCP1-positive fat, such as obese and elderly populations[46,47]. A potential caveat to consider is that the global activation of $Ca^{2+}$ cycling by SERCA2b or RyR2 would affect multiple metabolic organs because mutations in the *RYR2* gene mutations cause catecholaminergic polymorphic ventricular tachycardia and arrhythmogenic right ventricular cardiomyopathy type 2 (ref. 48,49). Hence, a critical assessment of the metabolic changes caused by adipose-specific manipulations of SERCA2b and RyR2 will be an important future avenue of study.

## Online Methods

### Animals

All animal experiments were performed under the guidelines established by the UCSF Institutional Animal Care and Use Committee. *Fabp4-Prdm16* transgenic mouse was reported previously[12,50]. *Fabp4-Prdm16* transgenic mouse and UCP1 null mice were backcrossed to the Bl6 background for more than eight generations. These mice were maintained on a regular chow or 60% HFD (Research Diets) with 12 hr light cycles. For generation of adipocyte-specific *Atp2a22−/−* mice, SERCA2 floxed mice were rederived using mouse sperm obtained from the *Atp2a2−/−* mice (C57BL/6N-*Atp2a2*$^{tm1a(EUCOMM)Hmgu}$). The sperms were obtained from the Medical Research Council Harwell and fertilized at the UCSF rederivation core facility. *Atp2a2*$^{flox/flox}$ mice were crossed to *Adipnectin*-Cre mice to generate the adipocyte-specific *Atp2a2−/−* mice. These mice were all in the Bl6 background. For cold exposure experiments, animals housed at 22°C were single-caged and subsequently exposed to 6°C. Mice were randomly assigned at the time of purchase or weaning to minimize any potential bias. Adipose tissues were fixed in 4% paraformaldehyde, followed by 70% ethanol until processing. Tissues were embedded in paraffin, sectioned at 5 μm, and stained with hematoxylin and eosin. Images were acquired with a DM2000 digital camera (Leica).

### Metabolic studies

Six-week-old animals (control, *Prdm16* Tg, *Ucp1*−/−, and *Prdm16* Tg x *Ucp1*−/− mice) were fed a HFD (D12492, Research Diet) or a regular diet (RD) under the ambient temperature at 22°C or thermoneutrality at 30°C for 12–24 weeks. HFD feedings were started at 6 weeks old. Body weight was measured every week. Whole-body energy expenditure ($VO_2$, $VCO_2$), food intake, and locomotor activity (beam break counts) were monitored using a Comprehensive Lab Animal Monitoring System (CLAMS, Columbus Instruments). CLAMS experiment in response to cold exposure was performed in mice at 10–12 weeks old under RD. Locomotor activity was measured by CLAMS for 5 days in mice at 12 weeks of HFD. Fat mass and lean mass were measured by the Body Composition Analyzer EcoMRI (Echo Medical Systems). For GTT experiments, mice were fed HFD or RD for 10 weeks. After an overnight fast, the mice were injected intraperitoneally with glucose (1.5 g/kg). For ITT experiments, the mice on HFD or for 11 weeks were injected intraperitoneally with insulin (0.75 U/kg for mice under HFD and 0.2U/kg for mice under RD) after 3 hours of fasting. Blood samples were collected at indicated time points, and glucose levels were measured using blood glucose test strips (Abbott).

### Temperature recording

Rectal temperature of the mice was monitored using a TH-5 thermometer (Physitemp). For tissue temperature recording, mice under anesthesia were implanted with the type T thermocouple probes at interscapular BAT, inguinal WAT, and skeletal muscle. Temperature in skeletal muscle on the back was record according to the previous study [51]. The temperature at each tissue was recorded by TC-2000 Meter (Sable Systems International). Core body temperature was maintained at 37°C or above. When tissue temperature reached stable, animals were treated with norepinephrine at a dose of 1 mg/kg.

### Electromyography (EMG)

Mice were placed in a restrainer to limit free movement and anesthetized with Avertin in prior to inserting the electrodes for EMG recording. Twenty nine-gauge needle electrodes were placed close to the back muscles near the neck. The EMG signal was processed (low-pass filter, 3 kHz; high-pass filter, 10 Hz; notch filter, 60 Hz) and amplified 1,000 x with Bio Amp (ADInstruments, Colorado Springs, CO). EMG data were collected from the implanted electrodes at a sampling rate of 2 kHz using LabChart 8 Pro Software (ADInstruments). The raw signal was converted to root mean square (RMS) activity. RMS activity was analyzed for shivering bursts in 10s windows.

### $^{18}$F-FDG-uptake assays

A total of 100 μCi of $^{18}$F-FDG was administered via tail vein under 2% isoflurane anesthesia. Mice were euthanized and dissected at 60 minutes following the $^{18}$F-FDG administration. Interscapular BAT, inguinal WAT, and epididymal WAT were collected and weighed. The radioactivity in the tissues was measured against known activity standards using a gamma-counter (Wizard 3; Perkin Elmer) at the UCSF Imaging Facility.

### PDH activity assays

Adipose tissue lysates were prepared by homogenizing tissues in ice-cold PBS buffer containing proteinase inhibitor cocktails. Five hundred μg of tissue lysates were applied to measure PDH enzymatic activities using the commercially available kit (Abcam, ab109902). PDH enzymatic activity was measured at 450 nm.

### RNA preparation and quantitative RT-PCR

Total RNA was extracted from adipose tissues and adipocytes using Trizol followed by the RNeasy mini-kit (Qiagen). cDNAs were synthesized by iScript (BioRad) following the protocol. qRT-PCR was performed using ABI ViiA™7 PCR machine. The primer sequences are listed in Supplementary Table 2.

### RNA-sequencing and bioinformatics

Sequencing libraries were constructed from total RNA as previously described [27]. High-throughput sequencing was performed using a HiSeq 2500 instrument (Illumina) at the UCLA Clinical Microarray Core. Raw reads for each library were mapped using TopHat version 2.0.8 against mouse (mm10) genome. The mapped reads were converted to FPKM (fragments per kilobase of exon per million fragments mapped) by running Cuffdiff 2.1.1 to determine gene expression. Biological pathway analysis was performed using Metascape[24]. The sequencing data were deposited in ArrayExpress (http://www.ebi.ac.uk/arrayexpress/) under accession number E-MTAB-4085.

### Metabolome analysis

Concentrations of all the charged metabolites were measured by capillary electrophoresis time-of-flight mass spectrometry (CE-TOFMS, Agilent Technologies, Santa Clara, CA) using the methods developed by the authors[52,53]. Briefly, to analyze cationic compounds, a fused silica capillary (50 um i.d. × 100 cm) was used with 1 M formic acid as the electrolyte[54]. Methanol/water (50% v/v) containing 0.1 *u*M hexakis(2,2-difluoroethoxy)phosphazene was delivered as the sheath liquid at 10 *u*l/min. ESI-TOFMS was performed in positive ion mode, and the capillary voltage was set at 4 kV. Automatic recalibration of each acquired spectrum was achieved using the masses of the reference standards ($[^{13}C$ isotopic ion of a protonated methanol dimer $(2MeOH+H)]^+$, $m/z$ 66.0632) and ([hexakis(2,2-difluoroethoxy)phosphazene $+H]^+$, $m/z$ 622.0290). To identify metabolites, relative migration times of all peaks were calculated by normalization to the reference compound, 3-aminopyrrolidine. The metabolites were identified by comparing their $m/z$ values and relative migration times to the metabolite standards. Quantification was performed by comparing their peak areas to calibration curves generated using internal standardization techniques with methionine sulphone. The other conditions were identical to those described previously[52]. To analyze anionic metabolites, a commercially available COSMO(+) (chemically coated with cationic polymer) capillary (50 *u*m i.d. x 105 cm) (Nacalai Tesque, Kyoto, Japan) was used with a 50 mM ammonium acetate solution (pH 8.5) as the electrolyte. Methanol/5 mM ammonium acetate (50% v/v) containing 0.1 uM hexakis(2,2-difluoroethoxy) phosphazene was delivered as the sheath liquid at 10 *u*l/min. ESI-TOFMS was performed in negative ion mode, and the capillary voltage was set at 3.5

kV. For anion analysis, trimesate and CAS were used as the reference and the internal standards, respectively. The other conditions were identical to those described previously[53]. Metabolomics analysis was performed by the authors who were blinded to the experimental groups.

## Cell culture

*Ucp1*−/− beige adipocyte line and brown adipocyte line were established by immortalizing the SVFs of the inguinal WAT and iBAT of *Prdm16* Tg x *Ucp1*−/− mice, respectively, according to the cell immortalization protocol using SV40 Large T antigen[27]. The SVFs from the subcutaneous WAT of neonatal piglets were immortalized using the same methodology. Clonal human beige adipocytes were previously reported[27]. Beige adipocyte differentiation was induced by treating confluent preadipocytes with DMEM containing 10% FBS, 0.5 mM isobutylmethylxanthine, 125 nM indomethacin, 2 μg $ml^{-1}$ dexamethasone, 850 nM insulin, and 1 nM T3, and 0.5 μM rosiglitazone. Two days after induction, cells were switched to the maintenance medium containing 10% FBS, 850 nM insulin, 1 nM T3, and 0.5 μM rosiglitazone. For cAMP treatment, cells were incubated with forskolin at a dose of 10 μM for 4 hours.

## DNA constructs for overexpression studies

Lentiviral mouse *Serca2b* ORF clone expression vector were obtained from GeneCopoeia (Ex-Mm28155-Lv207). DNA construct expressing RyR2 was a kind gift from Dr. Wayne Chen at University of Calgary. RyR2 cDNA was transfected into cells with Opti-mem medium using the Lipofectamine 2000 reagent, according to the manufacturer's instructions. Hygromycin at a dose of 200 μg/ml were used for selection. Calstabin2 (*FKBP1b*) was cloned to a retroviral vector (pMSCV) for retroviral expression. For retrovirus production, Phoenix packaging cells were transfected at 70% confluence by calcium phosphate method with 10 mg retroviral vectors. After 48 h, the viral supernatant was collected and filtered. Cells were incubated overnight with the viral supernatant and supplemented with polybrene.

## Gene silencing by lentivirus

Lentiviral shRNA expression vectors targeting mouse *Atp2a2* were obtained from GeneCopoeia (sh-#1, CS-MSH028715-33-LVRU6GH; sh-#2, CS-MSH028715-34-LVRU6GH-01, scrambled control, CSHCTR001-LVRU6GH). shRNA targeting pig *Atp2a2* (5-GAC TCT GCT TTG GAT TAT AAT-3′) was used to deplete SERCA2 in pig beige adipocytes. For lentivirus production, HEK293T packaging cells were transfected by calcium phosphate method with 10 μg lentiviral vectors and the packaging constructs (VSVg, pMDL, and Rev). After 48 hours, the viral supernatant was harvested and filtered. Immortalized preadipocytes derived from *Prdm16* Tg x *Ucp1*−/− mice were incubated overnight with the viral supernatant and supplemented with 6 μg/ml polybrene. Hygromycin at a dose of 200 μg/ml were used for selection.

## Gene deletion by the CRISPR/Cas9 system

Lentiviral vector (lentiCRISPR v2) was originally obtained from Addgene (#52961) and modified by replacing the puromycin selection cassette with the hygromycin B selection

cassette. The lentiviral vectors expressing guide RNA for *Atpa2a* (5′-GCA ATT TCC ACT ATA TCA CC-3′) and Cas9 were transfected in HEK293T packaging cells together with the packaging constructs (VSVg, pMDL, and Rev). As a control, lentiCRISPR vector expressing a scramble sequence (5′-GCA CTA CCA GAG CTA ACTC A-3′) was used. Immortalized preadipocytes derived from *Prdm16* Tg x *Ucp1*−/− mice were incubated with the above lentivirus and subsequently selected with 200 μg/ml hygromycin. We confirmed homozygous mutations in the *Atpa2a* genes by DNA sequencing in two independent clonal cell lines. In human beige adipocytes, the lentiviral vectors expressing guide RNA for *UCP1* (5′-CGG CCT CTA CGA CAC GGT CC-3′) was used to generate *UCP1*−/− human beige adipocytes.

### Glucose uptake assay

Differentiated beige adipocytes plated in a 12-well-plate incubated in serum-free medium for two hours. After wash in PBS, the cells were incubated in 1ml PBS containing 0.1 mM 2-deoxyglucose and 1 μCi/ml 2-deoxy-D-[$^{3}$H] glucose for 5 min. Subsequently, the cells were washed in cold PBS and harvested in 1% SDS. $^{3}$H-glucose uptake was detected by scintillation counter. Nonspecific deoxyglucose uptake is measured in the presence of 20 μM cytochalasin B and is subtracted from the total uptake to get specific glucose uptake. The values were normalized by protein concentrations as quantified by BCA method.

### Glucose oxidation assay

Differentiated beige adipocytes in a 6-well-plate incubated in a medium containing 0.5% FBS for two hours. After washed with PBS, the cells were incubated in 2ml KRB/HEPES buffer containing 5mM glucose, 2mM L-glutamine, 0.1 μCi/ml [1-$^{14}$C] glucose for 30 min at 37°C. $^{14}$C-carbon dioxide was trapped with filter papers by adding 300 μl of 1M benzothenium hydroxide to the filter papers and 350 μl of hydrogen peroxide to the wells. The Carbon dioxide trapped in the filter water was measured by scintillation counter.

### Fatty acid oxidation assay

Differentiated beige adipocytes plated in a 6-well-plate incubated in a medium containing 0.5% FBS for two hours. After washed in PBS, the cells were incubated in 2ml KRB/HEPES buffer containing 5mM glucose, 2mM L-glutamine, 0.5 μCi/ml, 500 μM [1-$^{14}$C]-Oleic acid bound to 0.7% BSA and Carnitine 100 μM for 2hr at 37°C.$^{14}$C-carbon dioxide trapped in the filter water was measured by scintillation counter.

### Immunocytostaining

Differentiated beige adipocytes were fixed with 4% paraformaldehyde for 15 minutes at RT, rinsed with PBS, and then exposed to 0.1% Triton X-100 and 2% BSA in PBS for 60 minutes. The cells were incubated with antibodies against SERCA2 (Thermo Fisher, 2A7-A1, 1:100), Calnexin (Santa Cruz, sc-11397, 1:100), or RyR2 polyclonal antibody (Thermo Fisher, PA5-36121, 1:200) overnight at 4°C. The slides were subsequently stained with secondary antibodies for one hour at room temperature and mounted in Vectashield (Vector Labs). Imaging was done using the Inverted Microscope Leica DMi8.

### Oxygen consumption assays

Oxygen consumption rate (OCR) in the interscapular BAT, inguinal WAT, and epididymal WAT was measured using the Seahorse XFe Extracellular Flux Analyzer (Agilent) in a 24-well-plate. The adipose tissues (0.5 mg for BAT, 1.5 mg for inguinal and epididymal WAT) were placed into XF24 Islet Capture Microplates and pre-incubated with assay media for one-hour in the presence or absence of norepinephrine. For cultured adipocytes, OCR and ECAR were measured in differentiated adipocytes that were treated with norepinephrine (1 μM), thapsigargin (2 μM), or agonists for α1-AR (Phenylephrine, 10 μM), α2-AR (Clonidine, 10 μM), β1-AR (Denopamine, 10 μM), and β3-AR (CL316,243, 1 μM) for one hour. Similarly, pharmacological inhibitors for α1-AR (phenoxybenzamine,10 μM) or beta3-AR (SR59230A,10 μM) were used. Ryanodine at 100 μM or ruthenium red at 1 μM were used in *Ucp1*−/−beige adipocytes. A cell-permeant $Ca^{2+}$ chelator, BAPTA, at 10 μM was added for two hours. Note that no cell death nor detach was observed after the BAPTA treatment. For the preparation of $Ca^{2+}$ depleted medium, EGTA at 1 mM was used. Cells were maintained in the XF assay medium supplemented with 1 mM sodium pyruvate, 2 mM GlutaMAXTM-I, and 25 mM glucose. Cells were subjected to the mitochondrial stress test by adding 2-DG (50 mM) or oligomycin (5 μM) followed by carbonyl cyanide 4-(trifluoromethoxy) phenylhydrazone (FCCP, 5 μM) and antimycin (5 μM). β-GPA at a dose of 50 mM was used to inhibit creatine cycling. When the assays required more than one plate, we combined multiple datasets and showed the results as % per controls.

### Intracellular $Ca^{2+}$ flux assays

Immortalized preadipocytes derived from inguinal WAT depots of wild-type mice and *Prdm16* Tg x *Ucp1*−/−mice were differentiated according to the adipocyte differentiation protocol as described above. Differentiated beige adipocytes were plated 30000 cells per well in 96-well plates one day before the assays. Intracellular $Ca^{2+}$ levels were determined by using the Fluo-8 No Wash Calcium Assay kit (Abcam, ab112129). Cells were incubated with Fluo-8 for 45min at room temperature in calcium free HHBS. Fluorescence intensity was quantified at Ex/Em = 490/525 nm.

### Immunoprecipitation and immunoblot

Protein lysates from adipose tissues were extracted using Qiagen TissueLyzer LT and NP-40 lysis buffer containing 50 mM Tris, pH 7.4, 150 mM NaCl, EDTA 5mM, 1% NP-40 and cOmplete protease inhibitors (Roche). The tissue lysates were immunoprecipitated using the antibody against SERCA2 (Thermo Fisher, 2A7-A1, 1:200). Mouse IgG was used to confirm the specificity of immunoprecipitation. The immunoprecipitants were subsequently applied for immunoblot using the SERCA2 antibody. β–actin (Sigma, A3854, 1:10,000) was used as loading control for each sample (input). Rabbit polyclonal PRDM16 antibody (1:1,000) was developed previously[12]. UCP1 antibodies for mouse (Abcam, ab10983, 1:1000) and human (Sigma, U6382, 1:1,000) were used to detect UCP1 proteins. Mitochondrial proteins were detected using MitoProfile® total OXPHOS rodent antibody cocktail (Abcam, ab110413, 1:1000).

### Statistics

Statistical analyses were performed using GraphPad Prism 7.0 (GraphPad Software, Inc., La Jolla, CA). All the data were represented as mean ± s.e.m. Where parametric tests were used, we checked normal distribution and difference of variable by Shapiro-Wilk test and F-test, respectively. When normal distribution was assumed, nonparametric method was used. A two-sample unpaired Student's *t*-test was used for two-group comparisons. One-way ANOVA followed by Tukey's test was used for multiple group comparisons. Two-way repeated-measures ANOVA followed by Fisher's LSD test was applied to determine the statistical difference in body-weight gain, glucose tolerance test, insulin tolerance test, and whole-body energy expenditure. *P* values below 0.05 were considered significant throughout the study. The sample size was determined based on our experience with the experimental models, anticipated biological variables, previous literatures, and also by a statistical power calculation (power = 0.8). We did not exclude samples or animals from the studies. RNA-sequencing, metabolomics, and histology were performed blinded. Other studies were not blinded.

### Data-availability statement

The data set generated during the current study is available from the corresponding author on reasonable request. A Life Science Reporting Summary is available.

## Supplementary Material

Refer to Web version on PubMed Central for supplementary material.

## Acknowledgments

We thank Dr. W. Chen at University of Calgary for providing the RyR2 overexpression construct. We are also grateful to Drs. C. Paillart for his support in the CLAMS studies, Y. Seo for his support in $^{18}$F-FDG-uptake assays, R. Zalpuri for technical assistance in EM analysis, K. Nakamura for his advice in tissue temperature recording, and to B.M. Spiegelman, E.T. Chouchani, and L. Kazak for their feedback. This work was supported by the NIH (DK97441 and DK108822), the Pew Charitable Trust, and Japan Science and Technology Agency to S.K., and by the AMED-CREST from the Japan Agency for Medical Research and Development, CREST from the Japan Science and Technology Agency and research funds from the Yamagata prefectural government and the City of Tsuruoka to T.S. We also acknowledge supports from the UCSF DERC (DK63720), the Yale MMPC (U2CDK059635) and DK40936. K.I. and K.T. are supported by the Manpei Suzuki Diabetes Foundation. Q.K. is supported by the China Scholarship Council (No.201506350063).

## References

1. Golozoubova V, et al. Only UCP1 can mediate adaptive nonshivering thermogenesis in the cold. FASEB J. 2001; 15:2048–2050. [PubMed: 11511509]
2. Nedergaard J, et al. UCP1: the only protein able to mediate adaptive non-shivering thermogenesis and metabolic inefficiency. Biochimica et biophysica acta. 2001; 1504:82–106. [PubMed: 11239487]
3. Kajimura S, Spiegelman BM, Seale P. Brown and Beige Fat: Physiological Roles beyond Heat Generation. Cell Metab. 2015; 22:546–559. [PubMed: 26445512]
4. Wu J, et al. Beige adipocytes are a distinct type of thermogenic fat cell in mouse and human. Cell. 2012; 150:366–376. [PubMed: 22796012]
5. Shabalina IG, et al. UCP1 in brite/beige adipose tissue mitochondria is functionally thermogenic. Cell reports. 2013; 5:1196–1203. [PubMed: 24290753]

6. Okamatsu-Ogura Y, et al. Thermogenic ability of uncoupling protein 1 in beige adipocytes in mice. PloS one. 2013; 8:e84229. [PubMed: 24386355]
7. Cinti, S. The adipose organ. Editrice Kurtis; Milano, Italy: 1999.
8. Petrovic N, et al. Chronic peroxisome proliferator-activated receptor gamma (PPARgamma) activation of epididymally derived white adipocyte cultures reveals a population of thermogenically competent, UCP1-containing adipocytes molecularly distinct from classic brown adipocytes. The Journal of biological chemistry. 2010; 285:7153–7164. [PubMed: 20028987]
9. Nedergaard J, Cannon B. UCP1 mRNA does not produce heat. Biochimica et biophysica acta. 2013; 1831:943–949. [PubMed: 23353596]
10. Xue B, et al. Genetic variability affects the development of brown adipocytes in white fat but not in interscapular brown fat. Journal of lipid research. 2007; 48:41–51. [PubMed: 17041251]
11. Guerra C, Koza RA, Yamashita H, Walsh K, Kozak LP. Emergence of brown adipocytes in white fat in mice is under genetic control. Effects on body weight and adiposity. The Journal of clinical investigation. 1998; 102:412–420. [PubMed: 9664083]
12. Seale P, et al. Prdm16 determines the thermogenic program of subcutaneous white adipose tissue in mice. J Clin Invest. 2011; 121:96–105. [PubMed: 21123942]
13. Shinoda K, et al. Phosphoproteomics Identifies CK2 as a Negative Regulator of Beige Adipocyte Thermogenesis and Energy Expenditure. Cell metabolism. 2015; 22:997–1008. [PubMed: 26525534]
14. McDonald ME, et al. Myocardin-related transcription factor a regulates conversion of progenitors to beige adipocytes. Cell. 2015; 160:105–118. [PubMed: 25579684]
15. Vegiopoulos A, et al. Cyclooxygenase-2 controls energy homeostasis in mice by de novo recruitment of brown adipocytes. Science (New York, N Y. 2010; 328:1158–1161.
16. Cohen P, et al. Ablation of PRDM16 and Beige Adipose Causes Metabolic Dysfunction and a Subcutaneous to Visceral Fat Switch. Cell. 2014; 156:304–316. [PubMed: 24439384]
17. Ohno H, Shinoda K, Ohyama K, Sharp LZ, Kajimura S. EHMT1 controls brown adipose cell fate and thermogenesis through the PRDM16 complex. Nature. 2013; 504:163–167. [PubMed: 24196706]
18. Ukropec J, Anunciado RP, Ravussin Y, Hulver MW, Kozak LP. UCP1-independent thermogenesis in white adipose tissue of cold-acclimated Ucp1−/− mice. The Journal of biological chemistry. 2006; 281:31894–31908. [PubMed: 16914547]
19. Granneman JG, Burnazi M, Zhu Z, Schwamb LA. White adipose tissue contributes to UCP1-independent thermogenesis. American journal of physiology. 2003; 285:E1230–1236. [PubMed: 12954594]
20. Rowland LA, Bal NC, Kozak LP, Periasamy M. Uncoupling Protein 1 and Sarcolipin Are Required to Maintain Optimal Thermogenesis and Loss of Both Systems Compromises Survival of Mice Under Cold Stress. The Journal of biological chemistry. 2015
21. Bal NC, et al. Sarcolipin is a newly identified regulator of muscle-based thermogenesis in mammals. Nature medicine. 2012; 18:1575–1579.
22. Kazak L, et al. A Creatine-Driven Substrate Cycle Enhances Energy Expenditure and Thermogenesis in Beige Fat. Cell. 2015; 163:643–655. [PubMed: 26496606]
23. Enerback S, et al. Mice lacking mitochondrial uncoupling protein are cold-sensitive but not obese. Nature. 1997; 387:90–94.
24. Tripathi S, et al. Meta- and Orthogonal Integration of Influenza “OMICs” Data Defines a Role for UBR4 in Virus Budding. Cell host & microbe. 2015; 18:723–735. [PubMed: 26651948]
25. Fujii J, et al. Identification of a mutation in porcine ryanodine receptor associated with malignant hyperthermia. Science (New York, NY. 1991; 253:448–451.
26. Quane KA, et al. Mutations in the ryanodine receptor gene in central core disease and malignant hyperthermia. Nature genetics. 1993; 5:51–55. [PubMed: 8220423]
27. Shinoda K, et al. Genetic and functional characterization of clonally derived adult human brown adipocytes. Nat Med. 2015; 21:389–394. [PubMed: 25774848]
28. Collins S. beta-Adrenoceptor Signaling Networks in Adipocytes for Recruiting Stored Fat and Energy Expenditure. Frontiers in endocrinology. 2011; 2:102. [PubMed: 22654837]

29. Fedorenko A, Lishko PV, Kirichok Y. Mechanism of fatty-acid-dependent UCP1 uncoupling in brown fat mitochondria. Cell. 2012; 151:400–413. [PubMed: 23063128]
30. Bertholet AM, et al. Mitochondrial Patch Clamp of Beige Adipocytes Reveals UCP1-Positive and UCP1-Negative Cells Both Exhibiting Futile Creatine Cycling. Cell metabolism. 2017; 25:811–822. e814. [PubMed: 28380374]
31. Lee SC, Nuccitelli R, Pappone PA. Adrenergically activated Ca2+ increases in brown fat cells: effects of Ca2+, K+, and K channel block. The American journal of physiology. 1993; 264:C217–228. [PubMed: 8430770]
32. Prestle J, et al. Overexpression of FK506-binding protein FKBP12.6 in cardiomyocytes reduces ryanodine receptor-mediated Ca(2+) leak from the sarcoplasmic reticulum and increases contractility. Circulation research. 2001; 88:188–194. [PubMed: 11157671]
33. Gomez AM, et al. FKBP12.6 overexpression decreases Ca2+ spark amplitude but enhances [Ca2+]i transient in rat cardiac myocytes. American journal of physiology. Heart and circulatory physiology. 2004; 287:H1987–1993. [PubMed: 15271664]
34. Loughrey CM, et al. Over-expression of FK506-binding protein FKBP12.6 alters excitation-contraction coupling in adult rabbit cardiomyocytes. The Journal of physiology. 2004; 556:919–934. [PubMed: 14966299]
35. Wehrens XH, et al. Protection from cardiac arrhythmia through ryanodine receptor-stabilizing protein calstabin2. Science (New York, NY. 2004; 304:292–296.
36. Santulli G, et al. Calcium release channel RyR2 regulates insulin release and glucose homeostasis. The Journal of clinical investigation. 2015; 125:1968–1978. [PubMed: 25844899]
37. Berg F, Gustafson U, Andersson L. The uncoupling protein 1 gene (UCP1) is disrupted in the pig lineage: a genetic explanation for poor thermoregulation in piglets. PLoS genetics. 2006; 2:e129. [PubMed: 16933999]
38. Denton RM. Regulation of mitochondrial dehydrogenases by calcium ions. Biochimica et biophysica acta. 2009; 1787:1309–1316. [PubMed: 19413950]
39. Marx SO, et al. PKA phosphorylation dissociates FKBP12.6 from the calcium release channel (ryanodine receptor): defective regulation in failing hearts. Cell. 2000; 101:365–376. [PubMed: 10830164]
40. Kramarova TV, et al. Mitochondrial ATP synthase levels in brown adipose tissue are governed by the c-Fo subunit P1 isoform. FASEB J. 2008; 22:55–63. [PubMed: 17666453]
41. Block BA. Thermogenesis in muscle. Annual review of physiology. 1994; 56:535–577.
42. Fu S, et al. Aberrant lipid metabolism disrupts calcium homeostasis causing liver endoplasmic reticulum stress in obesity. Nature. 2011; 473:528–531. [PubMed: 21532591]
43. Park SW, Zhou Y, Lee J, Lee J, Ozcan U. Sarco(endo)plasmic reticulum Ca2+-ATPase 2b is a major regulator of endoplasmic reticulum stress and glucose homeostasis in obesity. Proceedings of the National Academy of Sciences of the United States of America. 2010; 107:19320–19325. [PubMed: 20974941]
44. Tubbs E, et al. Mitochondria-associated endoplasmic reticulum membrane (MAM) integrity is required for insulin signaling and is implicated in hepatic insulin resistance. Diabetes. 2014; 63:3279–3294. [PubMed: 24947355]
45. Arruda AP, et al. Chronic enrichment of hepatic endoplasmic reticulum-mitochondria contact leads to mitochondrial dysfunction in obesity. Nature medicine. 2014; 20:1427–1435.
46. Yoneshiro T, et al. Age-related decrease in cold-activated brown adipose tissue and accumulation of body fat in healthy humans. Obesity (Silver Spring, Md. 2011; 19:1755–1760.
47. Saito M, et al. High incidence of metabolically active brown adipose tissue in healthy adult humans: effects of cold exposure and adiposity. Diabetes. 2009; 58:1526–1531. [PubMed: 19401428]
48. Tiso N, et al. Identification of mutations in the cardiac ryanodine receptor gene in families affected with arrhythmogenic right ventricular cardiomyopathy type 2 (ARVD2). Human molecular genetics. 2001; 10:189–194. [PubMed: 11159936]
49. Marks AR, Priori S, Memmi M, Kontula K, Laitinen PJ. Involvement of the cardiac ryanodine receptor/calcium release channel in catecholaminergic polymorphic ventricular tachycardia. Journal of cellular physiology. 2002; 190:1–6. [PubMed: 11807805]

50. Seale P, et al. Transcriptional control of brown fat determination by PRDM16. Cell metabolism. 2007; 6:38–54. [PubMed: 17618855]

51. Feketa VV, Balasubramanian A, Flores CM, Player MR, Marrelli SP. Shivering and tachycardic responses to external cooling in mice are substantially suppressed by TRPV1 activation but not by TRPM8 inhibition. American journal of physiology. Regulatory, integrative and comparative physiology. 2013; 305:R1040–1050.

52. Soga T, et al. Differential metabolomics reveals ophthalmic acid as an oxidative stress biomarker indicating hepatic glutathione consumption. The Journal of biological chemistry. 2006; 281:16768–16776. [PubMed: 16608839]

53. Soga T, et al. Metabolomic profiling of anionic metabolites by capillary electrophoresis mass spectrometry. Analytical chemistry. 2009; 81:6165–6174. [PubMed: 19522513]

54. Soga T, Heiger DN. Amino acid analysis by capillary electrophoresis electrospray ionization mass spectrometry. Analytical chemistry. 2000; 72:1236–1241. [PubMed: 10740865]

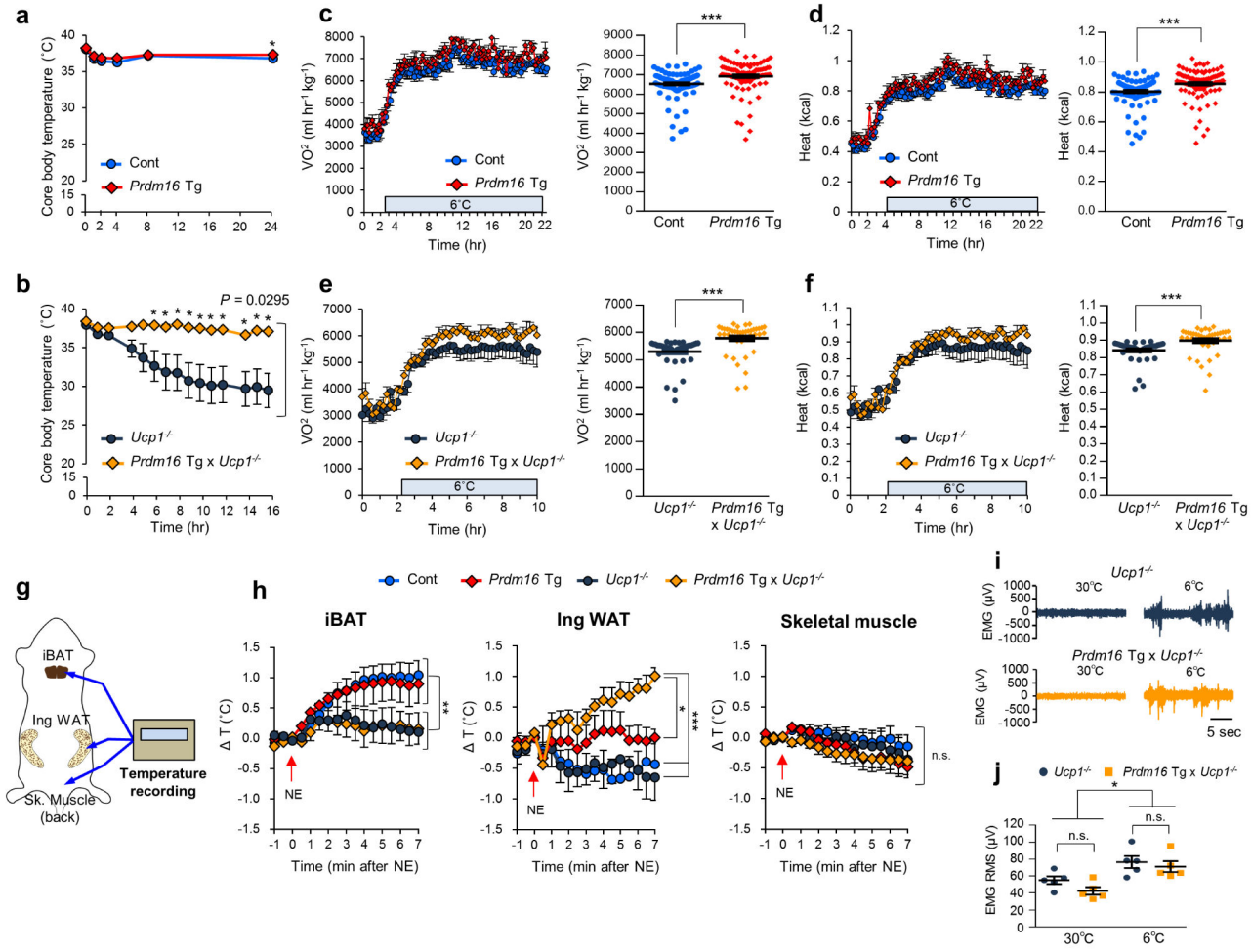


**Figure 1.**

UCP1 is dispensable for beige fat thermogenesis. (**a**) Rectal core body temperature of *Prdm16* Tg and the littermate controls (Cont) under 6°C at indicated time points. $n = 7$ for both genotypes. $^{*}P < 0.05$. (**b**) Rectal core body temperature of *Prdm16* Tg *x Ucp1−/−* and the littermate *Ucp1−/−* mice under 6 °C. *Ucp1−/−* mice, $n = 13$; *Prdm16 Tg x Ucp1−/−*, $n = 7$. (**c**) Whole-body oxygen consumption rate ($VO_2$) (left) and averaged $VO_2$ ± s.e.m. (right) of *Prdm16* Tg and the littermate controls following cold exposure at 6 °C. $n = 5$ for both groups. $^{***}P < 0.001$. (**d**) Whole-body heat generation (kcal) of the mice in **c**. $^{***}P < 0.001$. (**e**) Whole-body $VO_2$ of *Prdm16* Tg *x Ucp1−/−* and the littermate *Ucp1−/−* mice following cold exposure at 6 °C. $n = 5$ for both groups. $^{***}P < 0.001$. (**f**) Whole-body heat generation (kcal) of mice in **e**. $^{***}P < 0.001$. (**g**) Schematic diagram illustrating tissue temperature recording in the iBAT, the inguinal WAT, and the skeletal muscle. (**h**) Changes in tissue temperature ($\Delta T$) in the indicated tissues following NE treatment (arrows) in the indicated groups of mice. Control (Cont), $n = 6$; *Prdm16* Tg, $n = 4$; *Ucp1−/−*, $n = 5$; *Prdm16* Tg *x Ucp1−/−*, $n = 4$. $^{*}P < 0.05$, $^{**}P < 0.01$, $^{***}P < 0.001$. n.s., not significant. (**i**) Representative EMG traces. $n = 5$ for both groups. (**j**) The quantification converted to the root mean square (RMS) (i) of *Prdm16* Tg *x Ucp1−/−* and *Ucp1−/−* mice at 30°C and 6°C. $n = 5$ for both

groups. *$P < 0.05$. Data in (**a–f,h,j**) are expressed as means ± s.e.m. Data analyzed by Student's *t*-test (**a,c–f,j**) and ANOVA followed by Fisher's LSD test (**b**) or Tukey's test (**h**).

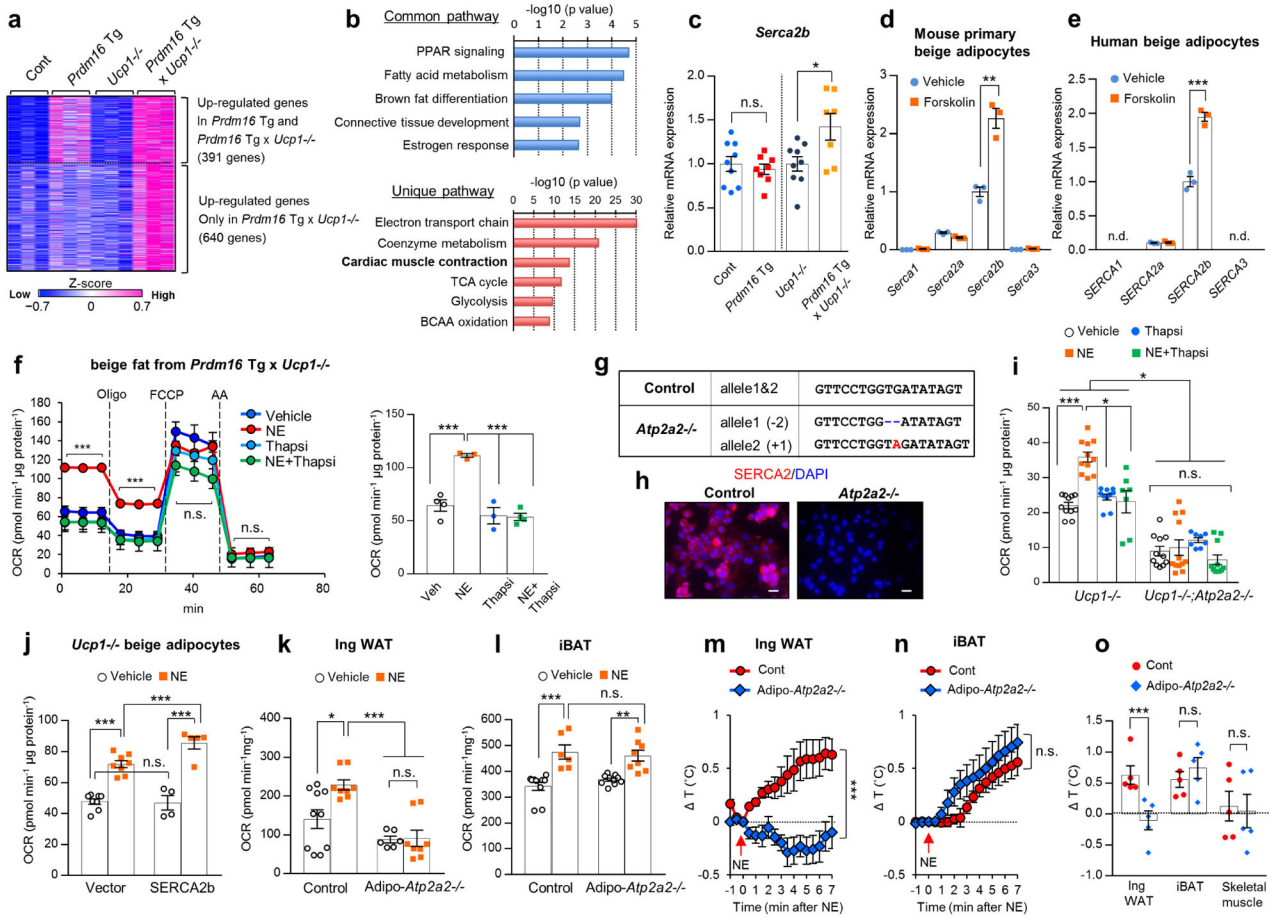


**Figure 2.**

SERCA2b controls UCP1-independent thermogenesis in beige fat. (**a**) Hierarchical clustering and heat-map of RNA-sequence data in the inguinal WAT. $n = 3$ for all groups. The color scale shows z-scored FPKM representing the mRNA level of each gene in blue (low expression)-white-red (high expression) scheme. (**b**) The commonly up-regulated pathways in *Prdm16* Tg mice and *Prdm16* Tg x *Ucp1*−/− mice relative to their littermate controls (up) and the uniquely up-regulated pathways in *Prdm16* Tg x *Ucp1*−/− mice relative to other genotypes (bottom). *P* values were shown on the top. $n = 3$ for all groups. (**c**) mRNA expression of *Serca2b* in the inguinal WAT. Control, $n = 9$; *Prdm16* Tg, $n = 8$; *Ucp1*−/−, $n = 9$; *Prdm16* Tg *x Ucp1*−/−, $n = 7$. $^{*}P < 0.05$. n.s., not significant. (**d**) mRNA expression of indicated genes in differentiated mouse primary beige adipocytes treated with forskolin or vehicle. $n = 3$ for both groups. $^{**}P < 0.01$. (**e**) mRNA expression of indicated genes in differentiated human beige adipocytes treated with forskolin or vehicle. $n = 3$ for both groups. $^{***}P < 0.001$. n.d., not detected. (**f**) OCR in *Ucp1*−/− beige adipocytes treated with vehicle, norepinephrine (NE), thapsigargin (thapsi), or NE plus thapsigargin. Oligomycin (Oligo), FCCP, and antimycin (AA) were added at indicated time points (left) and averaged basal OCR ± s.e.m (right). Vehicle, $n = 4$; NE, $n = 3$; Thapsi, $n = 3$; NE+Thapsi, $n = 4$. $^{***}P < 0.001$. (**g**) Genomic sequences of a clonal *Ucp1*−/− beige adipocyte line carrying the homozygous mutations in *Atp2a2* by the CRISPR-Cas9 system (*Atp2a2*−/−). Mutations

(red, insertion; -, deletion) and wild-type allele sequences (control) are shown. (**h**) SERCA2 immunohistochemistry in differentiated clonal *Ucp1*−/− beige adipocytes with homozygous mutations in *Atp2a2*−/− or control cells expressing a scrambled guide RNA. DAPI (blue) was used for nuclear staining. Scale bar= 25 μm. (**i**) Basal OCR in *Ucp1*−/− beige adipocytes expressing a control guide RNA (*Ucp1*−/−) and *Atp2a2*−/−;*Ucp1*−/− beige adipocytes. *Ucp1*−/− with vehicle and NE, $n = 11$ each; *Ucp1*−/− with Thapsi, $n = 10$; *Ucp1*−/− with NE +Thapsi, $n = 7$; *Atp2a2*−/−;*Ucp1*−/− with vehicle, $n = 11$; *Atp2a2*−/−;*Ucp1*−/− with NE, $n = 12$; *Atp2a2*−/−;*Ucp1*−/− with Thapsi, $n = 8$; *Atp2a2*−/−;*Ucp1*−/− with NE+Thapsi, $n = 11$. $^{*}P < 0.05$, $^{***}P < 0.001$. (**j**) Basal OCR in *Ucp1*−/− beige adipocytes expressing SERCA2b or an empty vector. Differentiated cells were treated with vehicle or NE for one hour. Control with vehicle and NE, $n = 8$ for both; SERCA2b with vehicle, $n = 4$; SERCA2b with NE, $n = 5$. $^{***}P < 0.001$. (**k**) OCR in the inguinal WAT of control and fat-specific *Atp2a2*−/− mice after tissue isolation and treatment with NE or vehicle for one hour. Control with vehicle, $n = 10$; with NE, $n = 8$; Adipo-*Atp2a2*−/− with vehicle, $n = 6$; with NE, $n = 8$. $^{*}P < 0.05$, $^{***}P < 0.001$. (**l**) OCR in the iBAT of control and fat-specific *Atp2a2*−/− mice. Control with vehicle, $n = 10$; with NE, $n = 6$; Adipo-*Atp2a2*−/− with vehicle, $n = 10$; with NE, $n = 8$. $^{**}P < 0.01$, $^{***}P < 0.001$. (**m**) Real-time changes in tissue temperature ($\Delta T$) in the inguinal WAT of control and Adipo-*Atp2a2*−/− mice following norepinephrine (NE) treatment. $n = 5$ for both groups. $^{***}P < 0.001$. (**n**) Real-time changes in tissue temperature ($\Delta T$) in the iBAT of mice in (m). (**o**) Quantification in tissues temperature change ($\Delta T$) in the indicated tissues of mice in (m). $^{***}P < 0.001$. Data in (**c–f,i–o**) are expressed as means ± s.e.m. Data analyzed by Student's *t*-test (**c–e,m–o**) and ANOVA followed by Tukey's test (**f,i–l**).

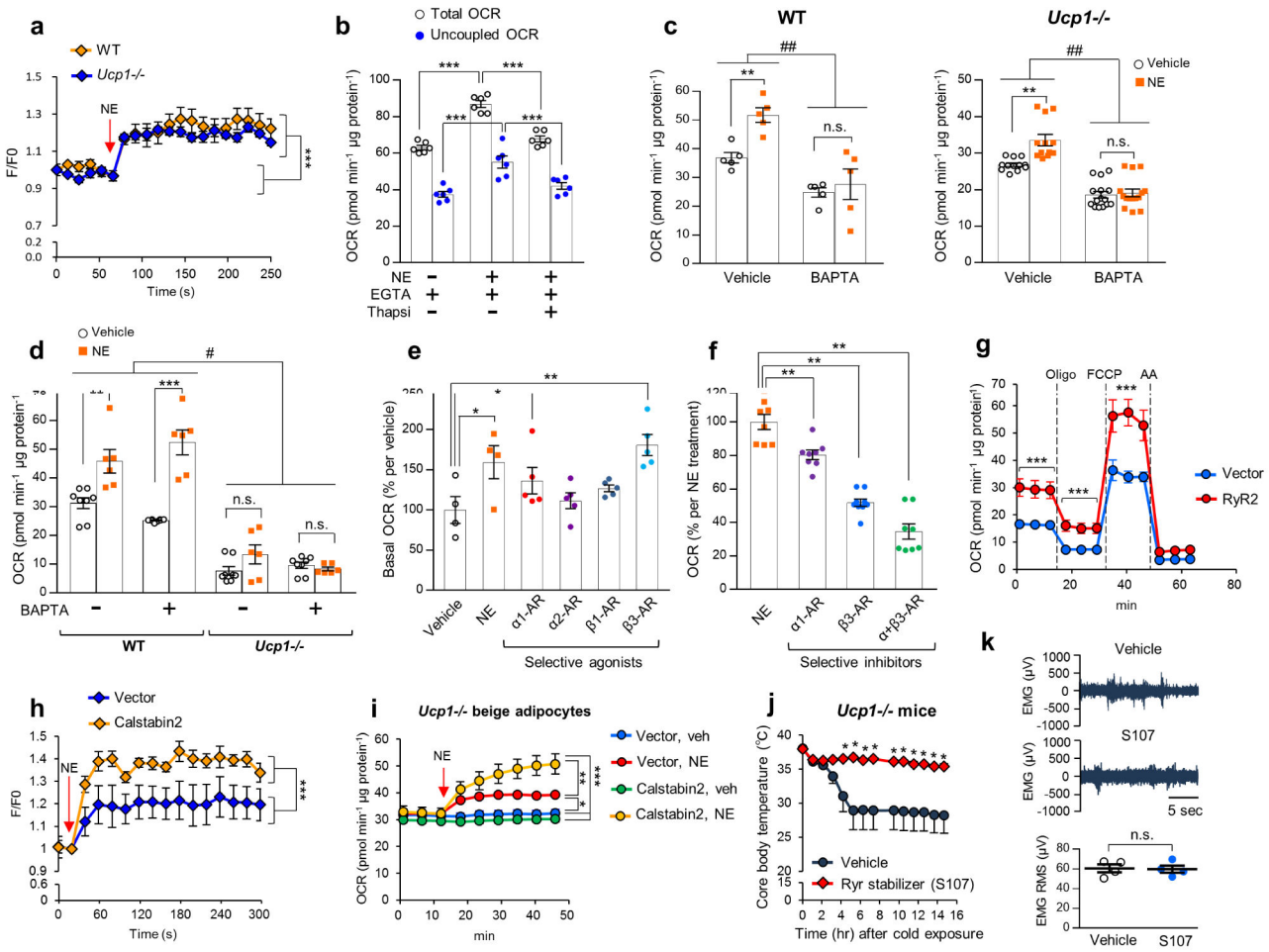


**Figure 3.**

Enhanced $Ca^{2+}$ cycling stimulates UCP1-independent thermogenesis in beige fat. (**a**) Intracellular $Ca^{2+}$ levels in differentiated beige adipocytes from wild-type (WT) and *Ucp1*−/− mice following NE treatment (arrow). $n = 6$ for all groups. ***$P < 0.001$ by NE treatment. (**b**) Basal and oligomycin-resistant (uncoupled) OCR in *Ucp1*−/− beige adipocytes in a $Ca^{2+}$ depleted medium containing EGTA in the presence of NE or thapsigargin (Thapsi). $n = 6$ for all groups. ***$P < 0.001$. (**c**) Basal OCR in WT and *Ucp1*−/− beige adipocytes treated with BAPTA or vehicle. WT cells, $n = 5$ for all the treatment; *Ucp1* −/− with vehicle or NE, $n = 12$; *Ucp1*−/− with BAPTA or BAPTA+NE, $n = 15$. **$P < 0.01$ between vehicle and NE, ##$P < 0.01$ between vehicle and BAPTA. n.s., not significant. (**d**) Basal OCR in WT and *Ucp1*−/− brown adipocytes incubated in a medium containing BAPTA or vehicle. WT with vehicle, $n = 8$; WT with NE, $n = 6$; WT with BAPTA, $n = 8$; WT with BAPTA+NE, $n = 6$; *Ucp1*−/− with vehicle $n = 8$; *Ucp1*−/− with NE, $n = 6$; *Ucp1*−/− with BAPTA, $n = 8$; *Ucp1*−/− with BAPTA+NE, $n = 6$. **$P < 0.01$, ***$P < 0.01$ between vehicle and NE, #$P < 0.05$ between WT and *Ucp1*−/−. (**e**) Basal OCR in *Ucp1*−/− beige adipocytes treated with NE or specific agonists for α1-AR (phenylephrine), α2-AR (clonidine), β1-AR (denopamine), and β3-AR (CL316243). Vehicle and NE, $n = 4$; phenylephrine, $n = 5$; clonidine, $n = 5$; denopamine, $n = 5$; CL316243, $n = 5$. *$P < 0.05$, **$P < 0.01$ relative to vehicle. (**f**) OCR in *Ucp1*−/− beige

adipocytes treated with specific inhibitors for α1-R (phenoxybenzamine) and β3-AR (SR59230A) in the presence of NE. NE, $n = 8$; phenoxybenzamine, $n = 8$; SR59230A, $n = 9$; phenoxybenzamine+SR59230A, $n = 8$. $^{**}P < 0.01$. (**g**) OCR in *Ucp1*−/− beige adipocytes expressing RyR2 or an empty vector. Oligomycin (Oligo), FCCP, and antimycin (AA) were added at indicated time points. $n = 5$ for all groups. $^{***}P < 0.001$. (**h**) NE-induced $Ca^{2+}$ release in *Ucp1*−/− beige adipocytes expressing Calbstabin2 or an empty vector in a $Ca^{2+}$ depleted medium. $n = 5$ for all groups. $^{***}P < 0.001$. (**i**) Basal OCR in *Ucp1*−/− beige adipocytes expressing Calbstabin2 or an empty vector. NE or vehicle was added at the indicated time point. Vector with vehicle $n = 8$; with NE, $n = 5$; Calstabin2 with vehicle and NE, $n = 10$ for both. $^{*}P < 0.05$, $^{**}P < 0.01$, $^{***}P < 0.001$. (**j**) Rectal core body temperature of *Ucp1−/−* mice treated with the RyR2 stabilizer S107 or vehicle under 6°C at indicated time points. Vehicle, $n = 9$; S107, $n = 8$. $^{*}P < 0.05$. (**k**) Representative EMG traces of *Ucp1−/−* mice treated with vehicle or S107 under 6°C. n=4 for both groups. Data are expressed as means ± s.e.m. Data analyzed by Student's *t*-test (**a,g,h,j,k**) and ANOVA followed by Tukey's test (**b–f,i**).

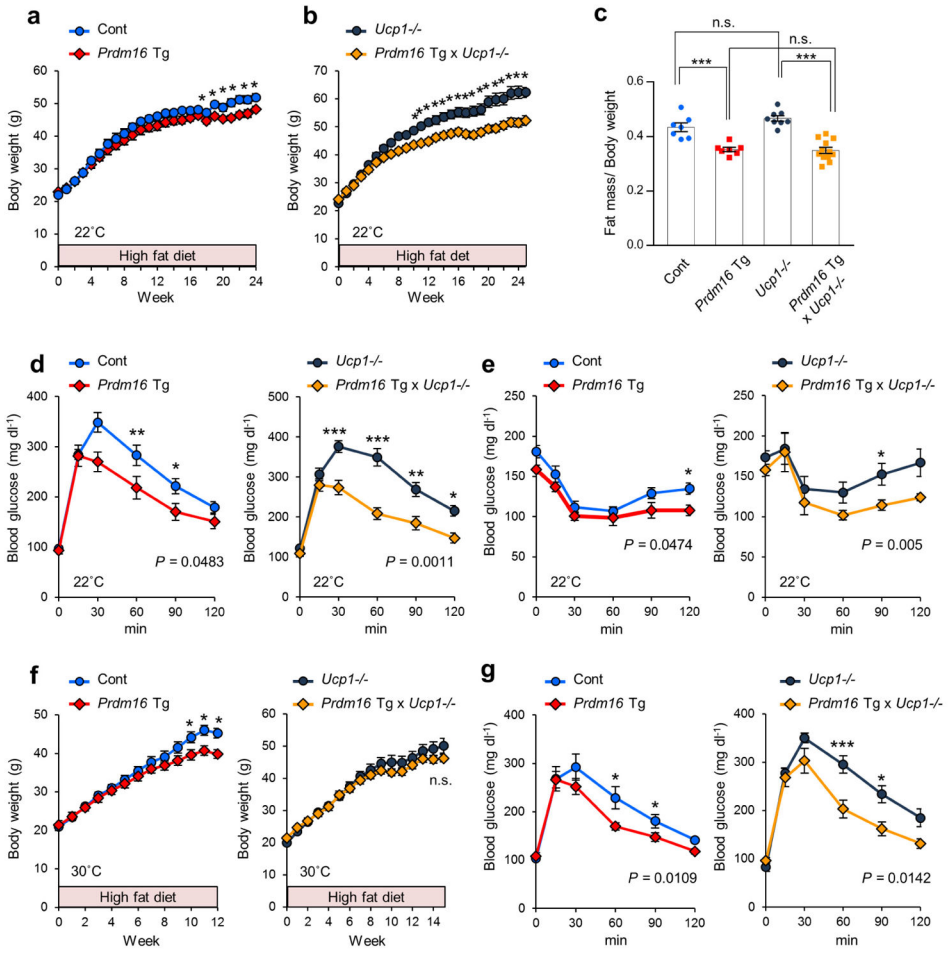


**Figure 4.**

UCP1-independent roles of beige fat in the regulation of body-weight and glucose metabolism *in vivo*. (**a**) Body-weight of *Prdm16* Tg mice and the littermate controls under HFD at 22°C. $n = 7$ for both groups. $*P < 0.05$. (**b**) Body-weight of *Prdm16* Tg x *Ucp1*−/− and the littermate *Ucp1*−/− mice under HFD at 22°C. *Ucp1*−/−, $n = 8$; *Prdm16* Tg *x Ucp1*−/−, $n = 12$. $*P < 0.05$. (**c**) Adiposity (fat mass per body-weight) of mice at 18 weeks of HFD. Control, $n = 7$; *Prdm16* Tg, $n = 7$; *Ucp1*−/−, $n = 8$; *Prdm16* Tg *x Ucp1*−/−, $n = 12$. $***P < 0.001$. n.s., not significant. (**d**) GTT in *Prdm16* Tg and the littermate controls (left) and *Prdm16* Tg x *Ucp1*−/− and the littermate *Ucp1*−/− mice (right) at 10 weeks of HFD at 22°C. Control, $n = 9$; *Prdm16* Tg, $n = 8$; *Ucp1*−/−, $n = 10$; *Prdm16* Tg *x Ucp1*−/−, $n = 7$. $*P < 0.05$, $**P < 0.01$, $***P < 0.001$. (**e**) ITT in mice in (d) at 11 weeks of HFD. $*P < 0.05$. (**f**) Body-weight of *Prdm16* Tg and the littermate controls (left) and *Prdm16* Tg x *Ucp1*−/− and the littermate *Ucp1*−/− mice (right) under HFD at 30°C. Control, $n = 9$; *Prdm16* Tg, $n = 7$; *Ucp1*−/−, $n = 7$; *Prdm16* Tg *x Ucp1*−/−, $n = 8$. $*P < 0.05$. (**g**) GTT in *Prdm16* Tg and the littermate controls (left) and *Prdm16* Tg x *Ucp1* −/− and the littermate *Ucp1*−/− mice (right) at 10 weeks of HFD under 30°C. Control, $n = 9$; *Prdm16* Tg, $n = 7$; *Ucp1*−/−, $n = 7$; *Prdm16* Tg *x Ucp1*−/−, $n = 5$. $*P < 0.05$, $***P < 0.001$. Data are expressed as means ± s.e.m. Data analyzed by Student's *t*-test (**c**) and ANOVA followed by Fisher's LSD test (**a,b,d–g**).

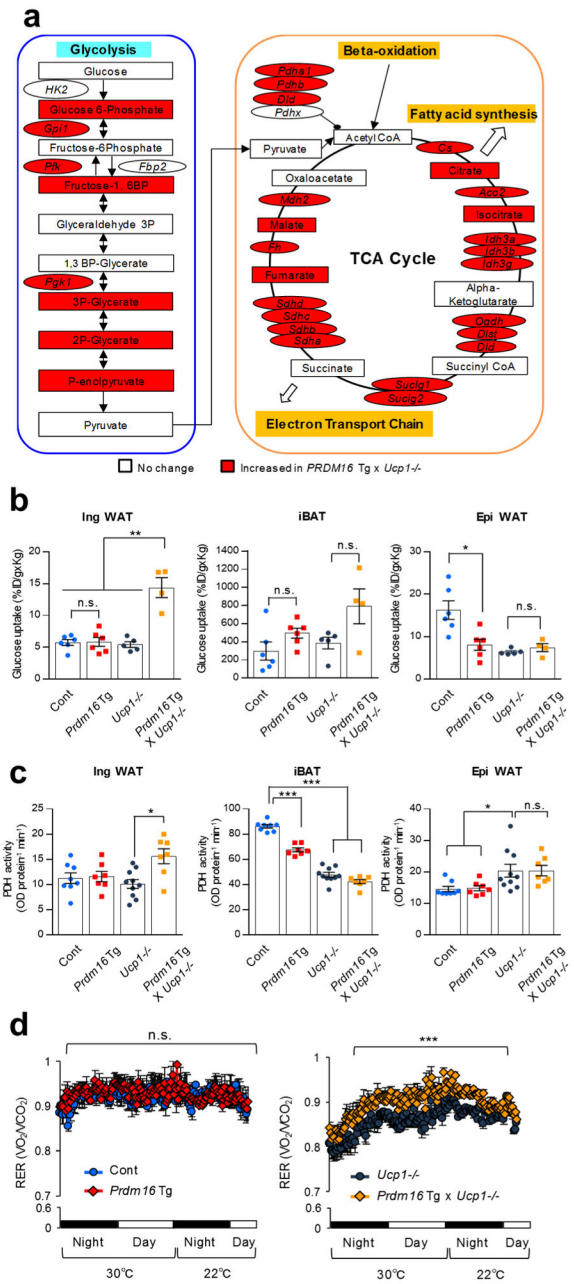


**Figure 5.**

Active glucose utilization in *Ucp1*−/− beige fat through enhanced glycolysis and TCA metabolism. (**a**) Enhanced metabolic pathways in the inguinal WAT of *Prdm16* Tg *x Ucp1*−/− mice. Based on RNA-sequencing and metabolomics, up-regulated genes and metabolites in the inguinal WAT of *Prdm16* Tg x *Ucp1*−/− mice are highlighted by red. $n = 3$ for all groups. (**b**) $^{18}$F-FDG uptake in the indicated tissues and groups of mice. Control (Cont), $n = 6$; *Prdm16* Tg, $n = 6$; *Ucp1*−/−, $n = 5$; *Prdm16* Tg *x Ucp1*−/−, $n = 4$. *$P < 0.05$, **$P < 0.01$. n.s., not significant. (**c**) PDH enzymatic activity in the indicated tissues and groups of mice. Control, $n = 8$; *Prdm16* Tg, $n = 7$; *Ucp1*−/−, $n = 10$; *Prdm16* Tg *x Ucp1*−/−, $n = 7$. *$P <$

0.05, ***$P < 0.001$. (**d**) Respiratory exchange ratio (RER, $VO_2/CO_2$) in mice under 30°C and 22°C. Mice were acclimated at 30°C for 5 days and moved to CLAMS. Control (Cont), $n = 6$; *Prdm16* Tg, $n = 5$; *Ucp1−/−*, $n = 6$; *Prdm16* Tg *x Ucp1−/−*, $n = 6$. ***$P < 0.001$. Data in (**b–d**) are expressed as means ± s.e.m. Data analyzed by Student's *t*-test (**a**) and ANOVA followed by Tukey's test (**b,c**) or Fisher's LSD test (**d**).

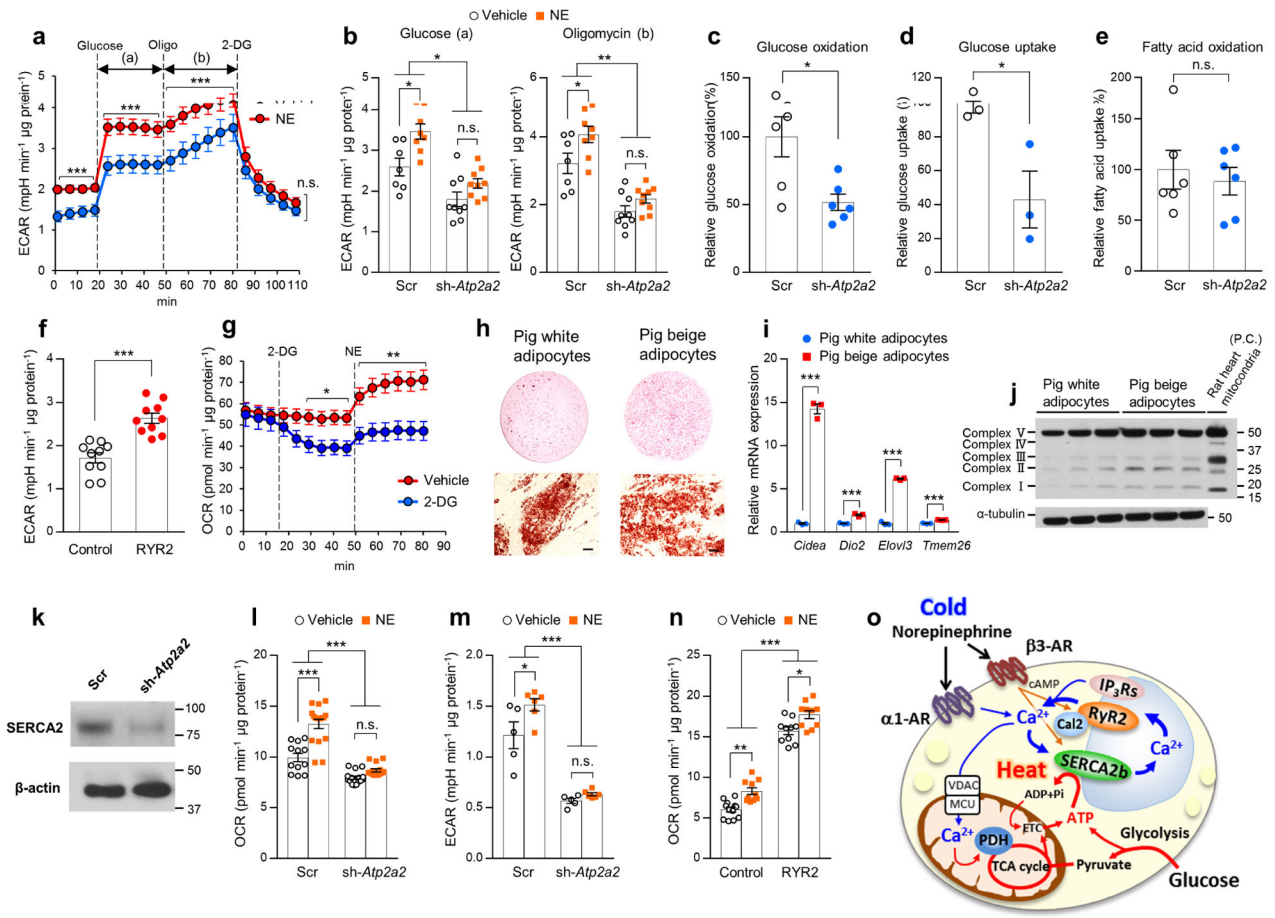


**Figure 6.**

The SERCA2-RyR2 pathway controls glucose utilization and thermogenesis in *Ucp1*−/− beige fat. (**a**) ECAR in *Ucp1*−/− beige adipocytes in the culture medium with low or high glucose concentrations. Glucose, oligomycin (Oligo), and 2-DG were added at indicated time points. Vehicle, $n = 7$; NE, $n = 8$. ***$P < 0.001$. (**b**) ECAR in *Ucp1*−/− beige adipocytes expressing a scrambled control RNA (Scr) or shRNA targeting *Atp2a2* (sh-*Atp2a2*). Differentiated cells were treated with NE or vehicle in the culture medium with a high glucose concentration (a) and oligomycin (b). Scr with vehicle, $n = 7$; Scr with NE, $n = 8$; sh-*Atp2a2*with vehicle, $n = 9$; sh-*Atp2a2* with NE, $n = 9$. *$P < 0.05$, **$P < 0.01$. (**c**) Glucose oxidation in *Ucp1*−/− beige adipocytes expressing a scrambled control RNA (Scr) or shRNA targeting *Atp2a2* (sh-*Atp2a2*). $n = 6$ for both groups. *$P < 0.05$. (**d**) Glucose uptake in *Ucp1*−/− beige adipocytes expressing a scrambled control RNA (Scr) or shRNA targeting *Atp2a2* (sh-*Atp2a2*). $n = 3$ for both groups. *$P < 0.05$. (**e**) Fatty acid oxidation in *Ucp1*−/− beige adipocytes expressing a scrambled control RNA (Scr) or shRNA targeting *Atp2a2* (sh-*Atp2a2*). $n = 6$ for both groups. n.s., not significant. (**f**) ECAR in *Ucp1*−/− beige adipocytes expressing RyR2 or an empty vector (Control). $n = 10$ for both groups. ***$P <$ 0.001. (**g**) OCR in *Ucp1*−/− beige adipocytes treated with 2-DG, NE, or oligomycin (Oligo) at indicated time points. Vehicle, $n = 9$; 2-DG, $n = 10$. *$P < 0.05$, **$P < 0.01$. (**h**) Oil-Red-O staining of differentiated pig adipocytes expressing PRDM16 (beige) and vector (white) at

low magnification (top) and high magnification (bottom). Scale bars, 50 μm. (**i**) mRNA expression of the indicated beige fat-selective genes in differentiated pig adipocytes expressing PRDM16 (beige) and an empty vector (white). $n = 3$ for both groups. ***$P <$ 0.001. (**j**) Mitochondrial OXPHOS proteins in differentiated pig adipocytes expressing PRDM16 (beige) and an empty vector (white). Tissue lysates from the rat heart were used as a positive control (P.C.). Immunoblot using the α-tublin antibody was shown as a loading control. Molecular weight (kDa) is shown on the right. (**k**) SERCA2 protein in differentiated pig beige adipocytes expressing a scrambled control RNA (Scr) or shRNA targeting *Atp2a2*. β-actin was shown as a loading control. (**l**) Basal OCR in pig beige adipocytes expressing a scrambled control RNA (Scr) or shRNA targeting *Atp2a2*. Scr with vehicle, $n = 12$; Scr with NE, $n = 17$; sh-*Serca2* with vehicle, $n = 15$; sh-*Serca2* with NE, $n = 15$. ***$P < 0.001$. (**m**) ECAR in pig beige adipocytes expressing a scrambled control RNA (Scr) or shRNA targeting *Atp2a2*. Scr with vehicle, $n = 5$; Scr with NE, $n = 6$; sh-*Serca2* with vehicle, $n = 5$; sh-*Serca2* with NE, $n = 6$. *$P < 0.05$, ***$P < 0.001$. (**n**) Basal OCR in pig beige adipocytes expressing RyR2 or an empty vector (Control). Control with vehicle, $n = 12$; Control with NE, RYR2 with vehicle, RYR2 with NE, $n = 10$. *$P < 0.05$, **$P < 0.01$, ***$P < 0.001$. (**o**) A proposed model of non-canonical thermogenesis in beige fat. A full explanation of the diagram is included in the Discussion section. The acronyms used in the diagram include adrenergic receptor (AR), sarco/endoplasmic reticulum $Ca^{2+}$-ATPase2b (SERCA2b), ryanodine receptor 2 (RyR2), inositol 1,4,5-trisphosphate receptors ($IP_3Rs$), calstabin2 (Cal2), voltage-dependent anion channel (VDAC), mitochondrial calcium uniporter (MCU), dehydrogenase (PDH), and mitochondrial electron transport chain (ETC). Data in (**a–g,i,l–n**) are expressed as means ± s.e.m. Data analyzed by Student's *t*-test (**a,c–g,i**) and ANOVA followed by Tukey's test (**b,l–n**).